Analysis of light neutrino exchange and short-range mechanisms in $0\nu\beta\beta$ decay

Frank F. Deppisch,[1,*] Lukas Graf,[2,†] Francesco Iachello,[3,‡] and Jenni Kotila[4,3,§]

[1]*Department of Physics and Astronomy, University College London, Gower Street, London WC1E 6BT, United Kingdom*
[2]*Max-Planck-Institut für Kernphysik, Saupfercheckweg 1, 69117 Heidelberg, Germany*
[3]*Center for Theoretical Physics, Sloane Physics Laboratory, Yale University, New Haven, Connecticut 06520-8120, USA*
[4]*Finnish Institute for Educational Research, University of Jyväskylä, P.O. Box 35, FI-40014 Jyväskylä, Finland*

(Received 3 October 2020; accepted 20 October 2020; published 16 November 2020)

Neutrinoless double beta decay ($0\nu\beta\beta$) is a crucial test for lepton number violation. Observation of this process would have fundamental implications for neutrino physics, theories beyond the Standard Model and cosmology. Focusing on so-called short-range operators of $0\nu\beta\beta$ and their potential interplay with the standard light Majorana neutrino exchange, we present the first complete calculation of the relevant nuclear matrix elements, performed within the interacting boson model (IBM-2). Furthermore, we calculate the relevant phase space factors using exact Dirac electron wave functions, taking into account the finite nuclear size and screening by the electron cloud. The obtained numerical results are presented together with up-to-date limits on the standard mass mechanism and effective $0\nu\beta\beta$ short-range operators in the interacting boson model framework. Finally, we interpret the limits in the particle physics scenarios incorporating heavy sterile neutrinos, left-right symmetry and R-parity violating supersymmetry.

DOI: 10.1103/PhysRevD.102.095016

I. INTRODUCTION

The nature of neutrinos and especially the origin of their masses are a crucial open question. While the Standard Model (SM) successfully explains the masses of the charged fermions it must be extended to incorporate neutrino masses. It would either require the presence of sterile neutrino states or effective lepton number violating (LNV) interactions. The first scenario allows the generation of *Dirac* neutrino masses analogous to those of the charged fermions. While certainly feasible, given the stringent upper limits $m_\nu \lesssim \mathcal{O}(0.1)$ eV on the absolute neutrino masses from Tritium decay [1,2] and cosmological observations [3], tiny Higgs Yukawa couplings are required. Also, total lepton number L will no longer be an accidental symmetry. Unless L symmetry is imposed, the sterile neutrinos would acquire an LNV *Majorana* mass. The most popular example for such a scenario is the seesaw mechanism where the sterile neutrinos have such a large Majorana mass $M \approx 10^{14}$ GeV naturally leading to light neutrino masses $m_\nu \approx 0.1$ eV [4–8].

High-scale seesaw mechanisms, or more generally scenarios where L is broken at very high scales, are not the only way to generate light Majorana neutrino masses; other possibilities include LNV at low scales in secluded sectors, at a higher loop order, and when allowing higher-dimensional effective interactions. If L-breaking occurs close to the electroweak scale, higher-dimensional LNV operators can be important. From a phenomenological point of view, searching for processes that violate total L thus play a crucial role in neutrino and beyond-the-SM (BSM) physics. We here focus on the search for $0\nu\beta\beta$ decay as the most sensitive approach to probe Majorana neutrino masses. Currently, the most stringent limit on the $0\nu\beta\beta$ decay half-life $T_{1/2}$ is set in the Germanium isotope $^{76}_{32}$Ge [9],

$$T_{1/2}(^{76}\mathrm{Ge}) \equiv T_{1/2}(^{76}_{32}\mathrm{Ge} \to {}^{76}_{34}\mathrm{Se} + e^- e^-) > 1.8 \times 10^{26}\ \mathrm{yr}. \tag{1}$$

However, Majorana neutrino masses are not the only contribution from BSM physics to $0\nu\beta\beta$ decay. We can generally consider the $0\nu\beta\beta$ decay rate by expressing high

*f.deppisch@ucl.ac.uk
†lukas.graf@mpi-hd.mpg.de
‡francesco.iachello@yale.edu
§jenni.kotila@jyu.fi

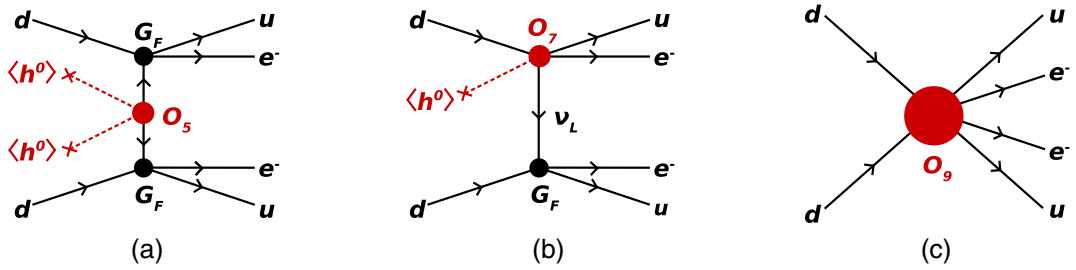

FIG. 1. Contributions to $0\nu\beta\beta$ decay from effective LNV operators. (a) Standard light neutrino exchange via dim-5 operator; (b) long-range contribution via dim-7 operator; (c) short-range contribution via dim-9 operator. Adapted from [26].

scale new physics contributions in terms of effective low-energy operators [10–13]. This only assumes that there are no exotic particles beyond the SM below the $0\nu\beta\beta$ energy scale of $m_F \approx 100$ MeV. In this paper, we concentrate on so called short-range operators and their interplay with the standard light Majorana neutrino mass mechanism. As context, we provide a brief overview of the possible mechanisms for $0\nu\beta\beta$ decay which can be categorized in two main classes:

(i) Long-range transitions via exchange of a light neutrino. This includes the so-called standard mass mechanism in Fig. 1(a), which is only possible if the neutrino is identical to its own antiparticle; i.e., if it is a Majorana fermion. The $0\nu\beta\beta$ decay rate can be estimated as $\Gamma^{0\nu\beta\beta}_{m_\nu} \sim m_\nu^2 G_F^4 m_F^2 Q^5_{\beta\beta} \sim (m_\nu/0.1\ \text{eV})^2 (10^{26}\ \text{yr})^{-1}$. Here, G_F is the SM Fermi coupling and the phase space scales as $Q^5_{\beta\beta}$ with the kinetic energy release $Q_{\beta\beta} = \mathcal{O}(1\ \text{MeV})$ for typical double beta decays. Specifically, the mass mechanism of $0\nu\beta\beta$ decay is sensitive to the effective neutrino mass $m_{\beta\beta} = \sum_i U_{ei}^2 m_{\nu_i}$, summing over the light Majorana neutrino masses m_{ν_i} weighted by the square of the charged-current leptonic mixing matrix elements U_{ei}. The inverse $0\nu\beta\beta$ decay half-life in a given isotope is then conventionally expressed as

$$T^{-1}_{1/2} = \frac{|m_{\beta\beta}|^2}{m_e^2} G_\nu |\mathcal{M}_\nu|^2, \tag{2}$$

with the phase space factor (PSF) G_ν and the nuclear matrix element (NME) $\mathcal{M}_\nu$. The normalization with respect to the electron mass m_e yields a small dimensionless parameter $|\epsilon_\nu| = |m_{\beta\beta}|/m_e$. The current bound in Eq. (1) sets a limit $|m_{\beta\beta}| \lesssim$ 79–180 meV at 90% confidence level (C.L.) for an unquenched axial coupling $g_A = 1.27$ [9], with the uncertainty mainly due to the NMEs in different nuclear models. Future experiments will probe $|m_{\beta\beta}| \approx 20$ meV [14], corresponding to the minimal value for inversely ordered neutrinos.

In BSM scenarios, a neutrino mass insertion is not necessarily required, cf. Fig. 1(b). In such cases, the decay rate is estimated as $\Gamma^{0\nu\beta\beta}_{\text{LR}} \sim v^2 \Lambda_{O_7}^{-6} G_F^2 m_F^4 Q^5_{\beta\beta} \sim (10^5\ \text{GeV}/\Lambda_{O_7})^6 \times (10^{26}\ \text{yr})^{-1}$, with the SM Higgs vacuum expectation value (VEV) $v = 246$ GeV and the scale Λ_{O_7} of the exotic dim-7 operator. Such long-range mechanisms via the exchange of light Majorana neutrinos with interactions beyond the SM have received considerable attention [15–20], as the suppression at dim-7 is still fairly low and $0\nu\beta\beta$ decay is sensitive to high scales. We note, though, that due to the neutrino helicity-flip intrinsic in the operator, typical mechanisms are suppressed by the light neutrino masses. It is generically difficult to have a dim-7 operator where the exotic long-range contribution dominates over the standard mass mechanism [21], though it can be achieved in ultraviolet complete theories with a modestly suppressed standard contribution [22–25].

(ii) Short-range contributions where all mediating particles are heavier than $m_F \approx 100$ MeV, cf. Fig. 1(c), are represented as contact interactions with six external fermions. These are the main focus of our analysis and they are generated by dim-9 and higher odd-dimensional operators. For a dim-9 operator, the decay rate can be estimated as $\Gamma^{0\nu\beta\beta}_{\text{SR}} \sim \Lambda_{O_9}^{-10} m_F^6 Q^5_{\beta\beta} \sim (5\ \text{TeV}/\Lambda_{O_9})^{10} (10^{26}\ \text{yr})^{-1}$, with the operator scale Λ_{O_9}. The inverse $0\nu\beta\beta$ decay half-life triggered by such a mechanism is expressed similarly to Eq. (2) as $T^{-1}_{1/2} = |\epsilon_I|^2 G_I |\mathcal{M}_I|^2$, with the PSF G_I and NME $\mathcal{M}_I$, both depending on the Lorentz structure of the effective operator. The coupling constant ϵ_I parametrizes the particle physics dynamics, i.e., the masses of the heavy states integrated out and their couplings. While such short-range contributions do not involve the exchange of light neutrinos at all, they still require the breaking of lepton number and the SM neutrinos will be of Majorana type. The short-range and standard mass mechanisms are thus expected to compete but the relative strength is highly dependent on the underlying model.

A detailed analytic derivation of the relevant NMEs for short-range operators was provided in our previous

paper [27], where we included additional NMEs that become important when the latest values of the nucleon form factors are taken into account. Moreover, we calculated PSFs using the exact radial wave functions and we presented the single electron energy and angular correlation distributions for the exotic short-range $0\nu\beta\beta$ decay mechanisms. In the present paper, we numerically evaluate all relevant NMEs within the interacting boson model (IBM-2) framework. This will allow us to set upper limits on the effective couplings ϵ_I where we will highlight the exchange of heavy sterile neutrinos as an important example. Within the same framework, we also provide updated NMEs for the standard light neutrino exchange and we analyse its interference with short-range mechanisms. The NMEs for the $0\nu\beta\beta$ transitions are generally difficult to calculate and the limits derived are affected for any contribution. Detailed treatments using different nuclear structure model approaches can be found in [28–37]. Despite tremendous efforts to improve the nuclear theory calculation, the latest matrix elements obtained using various approaches differ in many cases by factors of $\sim$(2–3).

The paper is organized as follows. We summarize the effective short-range Lagrangian at the quark level in Sec. II together with examples of underlying particle physics scenarios. The calculation of the $0\nu\beta\beta$ NMEs in the IBM-2 NME framework is outlined in Sec. III and that of the PSFs in Sec. IV. We then present our numerical results in Sec. V where we provide up-to-date limits on the standard mass mechanism and effective short-range $0\nu\beta\beta$ operators. Section VI concludes our discussion with a summary and an outlook.

II. SHORT-RANGE LNV OPERATORS AND NEUTRINO MASS MODELS

In general, new physics where lepton number is broken at a a high scale will induce SM effective operators of dimension five, seven, nine, and higher [38,39]. After electroweak symmetry breaking, this will give rise to long- and short-range contributions to $0\nu\beta\beta$ decay as outlined in the introduction, cf. Fig. 1. In this work we focus on short-range contributions and their potential interplay with the standard mass mechanism.

A. Effective Lagrangian

The general effective short-range interaction Lagrangian can be written in terms of five different Lorentz-invariant classes of fermion current products [11],

$$\mathcal{L}_{\rm SR} = \frac{G_F^2\cos^2\theta_C}{2m_p}\sum_{C_1,C_2,c}\Big(\epsilon_1^\chi J_{C_1}J_{C_2}j_c + \epsilon_2^\chi J_{C_1}^{\mu\nu}J_{C_2,\mu\nu}j_c + \epsilon_3^\chi J_{C_1}^{\mu}J_{C_2,\mu}j_c + \epsilon_4^\chi J_{C_1}^{\mu}J_{C_2,\mu\nu}j^\nu + \epsilon_5^\chi J_{C_1}^{\mu}J_{C_2}j_\mu\Big) + \text{H.c.}, \tag{3}$$

where the sum is over all unique combinations $\chi = \{C_1, C_2(,c)\}$ of chiralities $C_1, C_2, c = R, L$ of the quark and electron currents involved,

$$J_{R,L} = \bar{u}_a(1\pm\gamma_5)d_a, \qquad J^\mu_{R,L} = \bar{u}_a\gamma^\mu(1\pm\gamma_5)d_a, \qquad J^{\mu\nu}_{R,L} = \bar{u}_a\sigma_{\mu\nu}(1\pm\gamma_5)d_a, \tag{4}$$

$$j_{R,L} = \bar{e}(1\mp\gamma_5)e^c, \qquad j^\mu = \bar{e}\gamma^\mu\gamma_5 e^c. \tag{5}$$

Here, the four-component Dirac spinor operators representing the up quark, down quark, and electron are denoted by u, d, and e, respectively. Quark $SU(3)_C$ color indices are denoted by a, and each quark current forms a color singlet in our parametrization. As the lepton current must violate lepton number by two units, the charge conjugate electron field e^c appears there. Note that the chirality assignment in $j_{R,L}$ is flipped, i.e., the index L is associated with $1+\gamma_5$. This is due to the appearance of the charge-conjugated electron field and, for example, the operator $\bar{e}(1+\gamma_5)e^c$ describes the creation of two left-handed electrons. Furthermore, the usual definition $\sigma_{\mu\nu} = \frac{i}{2}[\gamma_\mu,\gamma_\nu]$ is used. The normalization of the Lagrangian by the factor $G_F^2\cos^2\theta_C/(2m_p)$ with the Fermi constant G_F, the SM Cabibbo angle θ_C and the proton mass m_p is conventional and results in dimensionless couplings ϵ_i^χ. In principle, each unique current combination will be associated with a separate coupling, $\epsilon_i^\chi = \epsilon_i^{C_1C_2(c)}$. Note that, in Ref. [11], the Lagrangian is defined without the factor $\cos^2\theta_C$. We chose to include it as the resulting PSFs can be defined in the same way as that for standard light neutrino exchange, cf. Sec. IV C.

Not all possible combinations of chiralities have to be considered in the Lagrangian Eq. (3), as redundancies and cancellations occur. First, the identity

$$[\bar{u}\sigma^{\mu\nu}(1+\gamma_5)d][\bar{u}\sigma_{\mu\nu}(1-\gamma_5)d] \equiv [\bar{u}\sigma^{\mu\nu}(1-\gamma_5)d][\bar{u}\sigma_{\mu\nu}(1+\gamma_5)d] = 0 \tag{6}$$

implies that terms corresponding to ϵ_2^{RLL}, ϵ_2^{LRL}, ϵ_2^{RLR}, and ϵ_2^{LRR} trivially vanish. Second, the Pauli exclusion principle dictates that $\bar{e}\gamma^\mu e^c = 0$ and $\bar{e}\sigma_{\mu\nu}(1\pm\gamma_5)e^c = 0$, and thus any operator containing vector, tensor, or axial-tensor electron currents can be omitted. Altogether, the short-range operators in Eq. (3) contain 24 independent nine-dimensional operators invariant under the broken SM gauge group $SU(3)_C\times U(1)_Q$ [27].

B. Example new physics scenarios with short-range contributions

To illustrate the generation of different short-range contributions, we consider three well-known scenarios beyond the SM.

1. Light and heavy neutrinos

As discussed in the introduction, the exchange of light active Majorana neutrinos is the most prominent mechanism for $0\nu\beta\beta$ decay. As a long-range contribution, it is not represented in the Lagrangian Eq. (3) but arises from the SM charged current

$$\mathcal{L} = \frac{G_F \cos\theta_C}{\sqrt{2}} [\bar{u}\gamma^\mu(1-\gamma_5)d] \sum_{i=1}^{3} U_{ei} [\bar{e}\gamma^\mu(1-\gamma_5)\nu_i] + \text{H.c.}. \tag{7}$$

The sum is over the three SM neutrino mass eigenstates ν_i, constructed as the Majorana spinors $\nu_i = \nu_{i,L} + \nu_{i,L}^c$ from the SM active left-handed neutrinos $\nu_{i,L}$ and their charge conjugates. This gives rise to the mass mechanism of $0\nu\beta\beta$ decay sensitive to the effective Majorana neutrino mass

$$m_{\beta\beta} = \sum_{i=1}^{3} U_{ei}^2 m_{\nu_i}. \tag{8}$$

The $0\nu\beta\beta$ decay half-life in a given isotope is then conventionally expressed as in Eq. (2).

One of the most attractive extensions of the SM involves adding fermionic states $\nu_{i,S}$ $(i = 1, \ldots, n_N)$ that are sterile under the SM gauge interactions. They can thus acquire (Dirac or Majorana type) masses without spoiling the SM gauge invariance and eventually mix with the SM neutrinos after electroweak symmetry breaking. We can again form Majorana states by constructing $N_i = \nu_{i,S} + \nu_{i,S}^c$. The sterile states participate in the leptonic charged current due to mixing with the active neutrinos,

$$\mathcal{L} = \frac{G_F \cos\theta_C}{\sqrt{2}} [\bar{u}\gamma^\mu(1-\gamma_5)d] \sum_{i=1}^{n_N} V_{eN_i} [\bar{e}\gamma^\mu(1-\gamma_5)N_i] + \text{H.c.}, \tag{9}$$

where V_{eN_i} are the elements of the active-sterile mixing matrix.

If the sterile neutrinos are much lighter than the nuclear physics scale $p_F \approx 100$ MeV, their contributions to $0\nu\beta\beta$ decay will be completely analogous to that of the active neutrinos and they can be included in Eq. (2) by replacing

$$m_{\beta\beta} \to m_{\beta\beta} + \sum_{i=1}^{n_N} V_{eN_i}^2 m_{N_i}, \quad (m_{N_i} \ll 100 \text{ MeV}). \tag{10}$$

Note that the U_{ei}, and hence $m_{\beta\beta}$, as well as the V_{eN_i} are in general complex numbers and cancellations can occur. In fact, if the Majorana states N_i are solely responsible for the light neutrinos masses in a Seesaw scenario, the active and sterile contributions cancel to zero.

If instead the sterile states are much heavier than the nuclear physics scale, $m_{N_i} \gg 100$ MeV, they can be integrated out, resulting in a contribution of the type $J_L^\mu J_{L,\mu} j_L$ and the associated coupling ϵ_3^{LLL} is matched with the underlying physics parameters as

$$\epsilon_3^{LLL} = \sum_{i=1}^{n_N} V_{eN_i}^2 \frac{m_p}{m_{N_i}}, \quad (m_{N_i} \gg 100 \text{ MeV}). \tag{11}$$

Note that the above considerations apply for sterile neutrinos that are Majorana fermions. This includes quasi-Dirac states that can be described by pairs of Majorana neutrinos (N_1, N_2) with a small mass splitting $|m_{N_1} - m_{N_2}| \ll m_{N_{1,2}}$ and a relative CP phase of $\pi/2$, $V_{eN_2} = iV_{eN_1} \Rightarrow V_{eN_2}^2 = -V_{eN_1}^2$. In the limit of Dirac sterile neutrinos with $m_{N_1} = m_{N_2}$, the contributions to $0\nu\beta\beta$ decay cancel.

2. Left-right symmetry

The minimal left-right symmetric model (LRSM) is based on the extended gauge symmetry $SU(3)_C \times SU(2)_L \times SU(2)_R \times U(1)_{B-L}$ [40–42]. It has a rich neutrino and $0\nu\beta\beta$ decay phenomenology as it naturally contains right-handed Majorana neutrinos N_i $(i = 1, 2, 3)$ that are charged under the $SU(2)_R$ part of the gauge group, forming a doublet together with the right-handed leptons. This gives rise to right-handed charged currents,

$$\mathcal{L} = \frac{g_R^2 \cos\theta_C^R}{8 m_{W_R}^2} [\bar{u}\gamma^\mu(1+\gamma_5)d] \sum_{i=1}^{3} U_{ei}^R [\bar{e}\gamma^\mu(1+\gamma_5)N_i] + \text{H.c.}, \tag{12}$$

mediated by a right-handed W_R boson with the gauge coupling strength g_R of the $SU(2)_R$ group. The angle θ_C^R and the mixing matrix U^R are the right-handed equivalents of the Cabibbo angle and the Pontecorvo–Maki–Nakagawa–Sakata matrix, respectively. The LRSM gauge group is understood to be spontaneously broken to that of the SM at a high scale giving masses to the right-handed W_R boson and neutrinos N_i. In turn, the active SM neutrino acquire masses via mixing with the heavy neutrinos (seesaw type I) as well as via the VEV of an electroweak triplet Higgs scalar present in the model (seesaw type II).

Hence, the standard light neutrino and the sterile heavy neutrino contribution described above are generally present. In addition, the equivalent diagram with a heavy neutrino and two W_R bosons contributes, giving rise to the short-range operator $J_R^\mu J_{R,\mu} j_R$ with $j_R = \bar{e}(1-\gamma_5)e^c$ associated with ϵ_3^{RRR} matched to the underlying physics parameters as

$$\epsilon_3^{RRR} = \frac{g_R^2}{g^2} f_{LR}^2 \sum_{i=1}^{3} (U_{ei}^R)^2 \frac{m_p}{m_{N_i}}, \quad \text{with}$$
$$f_{LR} = \frac{g_R}{g} \frac{\cos\theta_C^R}{\cos\theta_C} \frac{m_W^2}{m_{W_R}^2}, \tag{13}$$

where g is the SM $SU(2)_L$ gauge coupling strength. Note that the contribution is not suppressed by the small, light-heavy neutrino mixing but instead by the expectedly high W_R mass m_{W_R}. The right-handed mixing matrix U^R is approximately unitary with elements of order one, although cancellations due to complex phases can occur.

The SM W and the W_R boson are also expected to mix with an angle as large as $\sin\theta_{LR}^W \lesssim g_R m_W^2/(g m_{W_R}^2)$. This permits the right-handed lepton current to couple with a left-handed quark current mediated by the SM W giving rise to the contributions

$$\epsilon_3^{LRR} = \epsilon_3^{RLR} = \frac{\sin\theta_{LR}^W}{f_{LR}} \epsilon_3^{RRR}, \qquad \epsilon_3^{LLR} = \frac{\sin^2\theta_{LR}^W}{f_{LR}^2} \epsilon_3^{RRR}. \tag{14}$$

With the W mixing taking the generic value $\sin\theta_{LR}^W \approx g_R m_W^2/(g m_{W_R}^2) \approx f_{LR}$, all three effective couplings are of the same order. As mentioned, the LRSM also has the standard contribution from $m_{\beta\beta}$ and the sterile neutrino contribution ϵ_3^{LLL} in Eq. (11). In addition, the LRSM in principle also gives rise to the remaining contributions of type ϵ_3, namely $\epsilon_3^{LRL} = \epsilon_3^{RLL}$ and ϵ_3^{RRL} but these are suppressed by both the light-heavy neutrino mixing and the high W_R mass. Furthermore, the LRSM gives rise to additional long-range contributions that are not directly suppressed by the light neutrino masses.

Finally, the LRSM has contributions from the electroweak triplet scalars $\Delta_{L,R}$ that acquire VEVs v_R, $v_L \sim v^2/v_R$ during the spontaneous symmetry breaking, where v_R is the breaking scale of the left-right symmetry. This gives rise to a diagram to $0\nu\beta\beta$ decay mediated by two W_R bosons and the doubly charged scalars $\Delta_{L,R}^{--}$. Taking into account the W boson mixing, the contributions are

$$\epsilon_3^{RRR} = \frac{g_R^2}{g^2} f_{LR}^2 \sum_{i=1}^{3} (U_{ei}^R)^2 \frac{m_p m_{N_i}}{m_{\Delta_R^{++}}^2},$$
$$\epsilon_3^{LRR} = \epsilon_3^{RLR} = \frac{\sin\theta_{LR}^W}{f_{LR}} \epsilon_3^{RRR},$$
$$\epsilon_3^{LLR} = \frac{\sin^2\theta_{LR}^W}{f_{LR}^2} \epsilon_3^{RRR}, \tag{15}$$

analogous to Eqs. (13) and (14). Here, the heavy neutrino masses m_{N_i} appear because the couplings of the triplet Higgs to the gauge boson and electrons are proportional to v_R and the heavy neutrino Yukawa coupling, $m_N \sim y_N v_R$. Likewise, there are contributions from the left-handed Δ_L^{++} but they are additionally suppressed by the light neutrino masses (instead of m_{N_i}) and thus negligible.

3. R-parity violating supersymmetry

As the final example of an ultraviolet-complete theory, we consider the minimal supersymmetric Standard Model with R-parity violation [43,44]. Without explicitly imposing invariance under the discrete R symmetry where each field carries the multiplicative quantum number $R = (-1)^{3B+L+2S}$, with the baryon number B, total lepton number L, and spin S, the minimal supersymmetric Standard Model allows for the R-parity breaking terms,

$$W \supset \lambda_{ijk} L_i L_j \bar{E}_k + \lambda'_{ijk} L_i Q_j \bar{D}_k + \lambda''_{ijk} \bar{U}_i \bar{D}_j \bar{D}_k, \tag{16}$$

in the superpotential. Here, the indices i, j, k denote flavor generations of the superfields L, $\bar{E}$, Q, $\bar{D}$, and $\bar{U}$, associated with the SM weak lepton doublet L, the lepton singlet e^c, the quark doublet Q and the quark singlets d^c, u^c. Short-range contributions to $0\nu\beta\beta$ are induced by the second term in Eq. (16), namely that associated with λ'_{111} for the first lepton and quark generations [45]. They arise from diagrams with intermediate, heavy neutralinos, gluinos, squarks, and sleptons. The corresponding short-range Lagrangian is [46]

$$\mathcal{L}_{\rm SR} \supset \frac{G_F^2 \cos^2\theta_C}{2 m_p} (\epsilon_1^{RRL} J_R J_R + \epsilon_2^{RRL} J_R^{\mu\nu} J_{R,\mu\nu}) j_L, \tag{17}$$

i.e., a subset of the general short-range Lagrangian in Eq. (7) with scalar and tensor quark currents. The effective couplings ϵ_1^{RRL} and ϵ_2^{RRL} are generally functions of all supersymmetric particle masses and couplings involved. We here follow the assumptions of gluino dominance [46] where the diagrams involving gluinos and squarks contribute,

$$\epsilon_1^{RRL} = \frac{8\pi\alpha_s \lambda'^2_{111}}{9\cos^2\theta_C} \frac{G_F^{-2}}{m_{\tilde{q}}^4} \frac{m_p}{m_{\tilde{g}}}, \qquad \epsilon_2^{RRL} = -\frac{1}{8} \epsilon_1^{RRL}. \tag{18}$$

Here we also assume degeneracy of squark masses $m_{\tilde{q}} = m_{\tilde{u}_L} = m_{\tilde{d}_R}$ in line with Ref. [46]. In addition, $m_{\tilde{g}}$ is the gluino mass and $\alpha_s = 0.127$ is the strong fine structure constant at m_W. Note that the gluino dominance assumption is based on the relevant NME values and limits on supersymmetry particle masses from other sources and may thus not be appropriate in light of new results. We nevertheless adopt it for simplicity and to compare with Ref. [46].

III. DETERMINATION OF NUCLEAR MATRIX ELEMENTS

The NMEs for short-range mechanisms have been analytically derived in [27]. We follow the approach therein and summarize the basic formalism using nucleon form factors.

A. Nucleon form factors

The nucleon matrix elements of the colonr-singlet quark currents in Eq. (3) have the structure [47]

$$\langle p|\bar{u}(1\pm\gamma_5)d|n\rangle = \bar{N}\tau^+[F_S(q^2)\pm F_{P'}(q^2)\gamma_5]N', \tag{19}$$

$$\langle p|\bar{u}\gamma^\mu(1\pm\gamma_5)d|n\rangle = \bar{N}\tau^+\left[F_V(q^2)\gamma^\mu - i\frac{F_W(q^2)}{2m_p}\sigma^{\mu\nu}q_\nu\right]N' \pm \bar{N}\tau^+\left[F_A(q^2)\gamma^\mu\gamma_5 - \frac{F_P(q^2)}{2m_p}\gamma_5 q^\mu\right]N', \tag{20}$$

$$\langle p|\bar{u}\sigma^{\mu\nu}(1\pm\gamma_5)d|n\rangle = \bar{N}\tau^+\left[J^{\mu\nu}\pm\frac{i}{2}\epsilon^{\mu\nu\rho\sigma}J_{\rho\sigma}\right]N', \tag{21}$$

where τ^+ denotes the isospin-raising operator which converts a neutron into a proton, and the tensor $J^{\mu\nu}$ in Eq. (21) is defined as

$$J^{\mu\nu} = F_{T_1}(q^2)\sigma^{\mu\nu} + i\frac{F_{T_2}(q^2)}{m_p}(\gamma^\mu q^\nu - \gamma^\nu q^\mu) + \frac{F_{T_3}(q^2)}{m_p^2}(\sigma^{\mu\rho}q_\rho q^\nu - \sigma^{\nu\rho}q_\rho q^\mu). \tag{22}$$

The above matrix elements generally depend on the neutron and proton momenta $p_n = p_{N'}$ and $p_p = p_N$, respectively. The nucleon form factors are then functions of the momentum transfer $q = p_p - p_n$. The most general parametrization of the vector current in Eq. (20) would include also induced scalar and axial-tensor terms—these can be, however, safely neglected, since they vanish in the isospin-symmetric limit and they are not enhanced by any other effects [48].

The momentum dependence in Eqs. (19)–(21) is encoded in the nucleon form factors $F_X(q^2)$ with $X = S, P', V, W, A, P, T_1, T_2, T_3$, usually parametrized in the so-called dipole form, $F_X(q^2) = g_X/(1+q^2/m_X^2)^2$. Here, the so called charge g_X represents the value of the form factor at zero momentum transfer, $g_X \equiv F_X(0)$, and the scale m_X determines the shape of the form factor. We apply this parametrization to all form factors except for the pseudoscalar form factors $F_{P'}(q^2)$ and $F_P(q^2)$, which are enhanced by the pion resonance. The form factors with their corresponding parametrizations and charges are given by

$$F_S(q^2) = \frac{g_S}{(1+q^2/m_V^2)^2}, \qquad g_S = 1.0\ [49], \tag{23}$$

$$F_{P'}(q^2) = \frac{g_{P'}}{(1+q^2/m_V^2)^2}\frac{1}{1+q^2/m_\pi^2}, \qquad g_{P'} = 349\ [49], \tag{24}$$

$$F_V(q^2) = \frac{g_V}{(1+q^2/m_V^2)^2}, \qquad g_V = 1.0, \tag{25}$$

$$F_W(q^2) = \frac{g_W}{(1+q^2/m_V^2)^2}, \qquad g_W = 3.7, \tag{26}$$

$$F_A(q^2) = \frac{g_A}{(1+q^2/m_A^2)^2}, \qquad g_A = 1.269, \tag{27}$$

$$F_P(q^2) = \frac{g_P}{(1+q^2/m_A^2)^2}\frac{1}{1+q^2/m_\pi^2}, \quad g_P = 4g_A\frac{m_p^2}{m_\pi^2}\left(1-\frac{m_\pi^2}{m_A^2}\right) = 231\ [50], \tag{28}$$

$$F_{T_i}(q^2) = \frac{g_{T_i}}{(1+q^2/m_V^2)^2}, \quad g_{T_{1,2,3}} = 1.0, -3.3, 1.34\ [47]. \tag{29}$$

The shape parameters are $m_V = 0.84$ GeV, $m_A = 1.09$ GeV [49] and the pion mass is $m_\pi = 0.138$ GeV. The form factors $F_V(q^2)$, $F_W(q^2)$, and $F_A(q^2)$ can be determined experimentally and the parametrizations shown above provide a good description in the range $0 \le |q| \le 200$ MeV of interest in $0\nu\beta\beta$ decay. On the other hand, as it is not possible to directly obtain the induced pseudoscalar form factor from experiment, we use the parametrization suggested in Ref. [50], which is based on the partially conserved axial-vector current hypothesis. The corresponding value of the free g_P charge agrees with the recent chiral perturbation theory analysis [51], which yields the value $g_P = 233$. The value is also consistent with measurements of muon capture. With the muon mass $m_\mu = 0.105$ GeV, the resulting value of $F_P(-0.88m_\mu^2) = 8.0$ agrees well with the measured value of $F_P(-0.88m_\mu^2) = 8.06 \pm 0.55$ [52]. The scalar and pseudoscalar charges, g_S and $g_{P'}$, come from recent lattice QCD calculations [53]. As there is not much information on the q^2 dependence of the corresponding form factors, we use the dipole parametrization, which, in the Breit frame, is the Fourier transform of the matter distribution. In the case of the pseudoscalar form factor we also include the monopole factor $1/(1+q^2/m_\pi^2)$ used in chiral perturbation theory. As for the tensor form factors, only F_{T_1} enters our calculations. The value of the corresponding charge g_{T_1} quoted by Ref. [53] reads 0.987 ± 0.055. We emphasize that the charges in Eqs. (23)–(29) are applicable at the free nucleon level. When calculating the $0\nu\beta\beta$ decay NMEs, we will use an

effective axial-vector charge $g_A = 1.0$ and, consequently, an induced pseudoscalar charge $g_P(g_A = 1.0) = 182$ to approximately account for quenching in the nuclear medium.

B. Nuclear matrix elements

The five different types of quark current products appearing in Eq. (3) are mapped to the nucleon matrix elements according to Eqs. (19)–(21). By virtue of a nonrelativistic expansion and the closure approximation, the resulting product of nucleon matrix elements is then mapped to the *nuclear* matrix element between the final and initial 0^+ nuclear states involved in the $0\nu\beta\beta$ decay. This procedure is described in Ref. [27], and we here summarize the definition of NMEs involved. One should note that in the following expressions the relative sign between Gamow-Teller (GT) and tensor (T) terms is different than in our previous papers [28–30,54] and other available literature taking into account tensor terms using the formulation in [50]. The confusion about the relative sign arises from Eqs. (13) and (22) in [50], where in Eq. (13) a minus sign is used in front of the tensor term, while in Eq. (22) the plus sign is used. The tensor term contributes very little to the standard long-range mechanism, but, in the case of short-range mechanisms, it has a notable effect. Thus we have checked the derivation and concluded that the following signs should be used.

The NMEs for the five short-range operators will generally depend on the chiralities of the two quark currents involved. For the first three operators associated with ϵ_1^χ, ϵ_2^χ, and ϵ_3^χ, the two quark currents are of the same type. Consequently, three possible combinations occur corresponding to the chiralities RR, LL, and $(RL + LR)/2$. It turns out that the resulting NMEs only depend on whether the quark chiralities are equal (RR, LL) or different $(RL + LR)/2$, represented by the upper and lower sign, respectively, in the expressions

$$\mathcal{M}_1 = g_S^2 \mathcal{M}_F \pm \frac{g_{P'}^2}{12}(\mathcal{M}_{\rm GT}^{\prime P'P'} + \mathcal{M}_T^{\prime P'P'}), \tag{30}$$

$$\mathcal{M}_2 = -2 g_{T_1}^2 \mathcal{M}_{\rm GT}^{T_1 T_1}, \tag{31}$$

$$\begin{aligned}\mathcal{M}_3 = {} & g_V^2 \mathcal{M}_F + \frac{(g_V + g_W)^2}{12}(-2\mathcal{M}_{\rm GT}^{\prime WW} + \mathcal{M}_T^{\prime WW}) \\ & \mp \left[g_A^2 \mathcal{M}_{\rm GT}^{AA} - \frac{g_A g_P}{6}(\mathcal{M}_{\rm GT}^{\prime AP} + \mathcal{M}_T^{\prime AP}) \right. \\ & \left. + \frac{g_P^2}{48}(\mathcal{M}_{\rm GT}^{\prime\prime PP} + \mathcal{M}_T^{\prime\prime PP}) \right].\end{aligned} \tag{32}$$

For the operators associated with ϵ_4^χ and ϵ_5^χ, the two quark currents involved have different Lorentz structures and thus all four possible combinations of chiralities have to be considered in principle: RR, LL, RL, and LR. Again, it turns out that the NMEs only distinguish between the case where the quark chiralities are the same (RR, $LL \to$ upper sign) or different (RL, $LR \to$ lower sign),

$$\mathcal{M}_4 = \mp i \left[g_A g_{T_1} \mathcal{M}_{\rm GT}^{AT_1} - \frac{g_P g_{T_1}}{12}(\mathcal{M}_{\rm GT}^{\prime PT_1} + \mathcal{M}_T^{\prime PT_1}) \right], \tag{33}$$

$$\begin{aligned}\mathcal{M}_5 = {} & g_V g_S \mathcal{M}_F \pm \left[\frac{g_A g_{P'}}{12}(\tilde{\mathcal{M}}_{\rm GT}^{AP'} + \tilde{\mathcal{M}}_T^{AP'}) \right. \\ & \left. - \frac{g_P g_{P'}}{24}(\mathcal{M}_{\rm GT}^{\prime q_0 PP'} + \mathcal{M}_T^{\prime q_0 PP'}) \right].\end{aligned} \tag{34}$$

In the above expressions, we have explicitly factored the form factor charges $g_X = F_X(0)$. The q dependence arising from the product of the reduced form factors $F_X(q^2)/g_X$ is still to be included in the various matrix elements appearing in Eqs. (30)–(34). The individual Fermi ($\mathcal{M}_F$), Gamow-Teller ($\mathcal{M}_{\rm GT}$), and tensor ($\mathcal{M}_T$) NMEs along with the associated reduced form factor products $\tilde{h}(q^2)$ are given in Table I. The numerical values of these NME will be given in Sec. III C, but we would like to note that the so-called recoil NMEs, $\tilde{\mathcal{M}}_{\rm GT}^{AP}$ and $\tilde{\mathcal{M}}_T^{AP}$, and the NMEs explicitly depending on the temporal momentum transfer q_0, $\mathcal{M}_{\rm GT}^{\prime q_0 PP}$, $\mathcal{M}_T^{\prime q_0 PP}$ are difficult to evaluate exactly. We instead assume that the sum of nucleon spatial momenta is $\mathbf{Q} = \mathbf{p}_a + \mathbf{p}_b \approx \mathbf{q}$ [15–17], approximately applicable in an average sense considering that the NME is calculated summing over all nucleons in the nucleus. Similarly, we take the average value $q_0 \sim \mathbf{q}^2/m_p \approx 10$ MeV [17] for the temporal component of the momentum transfer. This allows us to reduce the corresponding NMEs as indicated in Table I.

In addition to the product of the reduced nucleon form factors, the NMEs listed in Table I also contain the so-called neutrino potential describing the q dependence of the underlying particle physics mediator of $0\nu\beta\beta$ decay. Here we follow the formulation of [29,50] where the two-body transition operator is constructed in momentum space as the product of the neutrino potential $v(q)$ times the product of the reduced form factors $\tilde{h}(q^2)$. In the case of the short-range mechanisms we consider here, the neutrino potential is especially simple; as pointlike operators, they are described by a Dirac delta function in configuration space, $\delta(\mathbf{r}_a - \mathbf{r}_b)$, hence in momentum space it is a q-independent constant. Following the usual normalization the short-range neutrino potential is [29,50]

$$v(q^2) = \frac{2}{\pi}\frac{1}{m_e m_p}. \tag{35}$$

We also consider the standard light neutrino exchange mechanism with the NME

TABLE I. Double beta decay Fermi ($\mathcal{M}_F$), Gamow-Teller ($\mathcal{M}_{\rm GT}$), and tensor ($\mathcal{M}_T$) NMEs appearing in Eqs. (30)–(34), with the associated reduced form factor product $\tilde{h}(q^2)$. The NMEs are calculated using the functions $h_\circ(q^2) = v(q^2)\tilde{h}_\circ(q^2)$ enhanced by the neutrino potential Eq. (35) for short-range mechanisms and standard light neutrino exchange, Eq. (37). The subscript X stands for $X = V, W, T_1$, for which the same form factor shape parameter m_V applies. The Pauli matrices in the space of the spins of the individual nucleons a, b are represented as $\boldsymbol{\sigma}_{a,b}$ and the tensor NMEs are calculated over $S_{ab} = 3(\boldsymbol{\sigma}_a \cdot \mathbf{q})(\boldsymbol{\sigma}_b \cdot \mathbf{q}) - (\boldsymbol{\sigma}_a \cdot \boldsymbol{\sigma}_b)$.

NME	$\tilde{h}_\circ(q^2)$
$\mathcal{M}_F = \langle h_{XX}(q^2)\rangle$	$\tilde{h}_{XX}(q^2) = \frac{1}{(1+q^2/m_V^2)^4}$
$\mathcal{M}_{\rm GT}^{\prime P'P'} = \langle \frac{\mathbf{q}^2}{m_p^2} h_{PP}(q^2)(\boldsymbol{\sigma}_a \cdot \boldsymbol{\sigma}_b)\rangle$	$\tilde{h}_{PP}(q^2) = \frac{1}{(1+q^2/m_A^2)^4}\frac{1}{(1+q^2/m_\pi^2)^2}$
$\mathcal{M}_T^{\prime P'P'} = \langle \frac{\mathbf{q}^2}{m_p^2} h_{PP}(q^2) S_{ab}\rangle$	$\tilde{h}_{PP}(q^2)$
$\mathcal{M}_{\rm GT}^{T_1T_1} = \langle h_{XX}(q^2)(\boldsymbol{\sigma}_a \cdot \boldsymbol{\sigma}_b)\rangle$	$\tilde{h}_{XX}(q^2)$
$\mathcal{M}_{\rm GT}^{\prime WW} = \langle \frac{\mathbf{q}^2}{m_p^2} h_{XX}(q^2)(\boldsymbol{\sigma}_a \cdot \boldsymbol{\sigma}_b)\rangle$	$\tilde{h}_{XX}(q^2)$
$\mathcal{M}_T^{\prime WW} = \langle \frac{\mathbf{q}^2}{m_p^2} h_{XX}(q^2) S_{ab}\rangle$	$\tilde{h}_{XX}(q^2)$
$\mathcal{M}_{\rm GT}^{AA} = \langle h_{AA}(q^2)(\boldsymbol{\sigma}_a \cdot \boldsymbol{\sigma}_b)\rangle$	$\tilde{h}_{AA}(q^2) = \frac{1}{(1+q^2/m_A^2)^4}$
$\mathcal{M}_{\rm GT}^{\prime AP} = \langle \frac{\mathbf{q}^2}{m_p^2} h_{AP}(q^2)(\boldsymbol{\sigma}_a \cdot \boldsymbol{\sigma}_b)\rangle$	$\tilde{h}_{AP}(q^2) = \frac{1}{(1+q^2/m_A^2)^4}\frac{1}{1+q^2/m_\pi^2}$
$\mathcal{M}_T^{\prime AP} = \langle \frac{\mathbf{q}^2}{m_p^2} h_{AP}(q^2) S_{ab}\rangle$	$\tilde{h}_{AP}(q^2)$
$\mathcal{M}_{\rm GT}^{\prime\prime PP} = \langle \frac{\mathbf{q}^4}{m_p^4} h_{PP}(q^2)(\boldsymbol{\sigma}_a \cdot \boldsymbol{\sigma}_b)\rangle$	$\tilde{h}_{PP}(q^2)$
$\mathcal{M}_T^{\prime\prime PP} = \langle \frac{\mathbf{q}^4}{m_p^4} h_{PP}(q^2) S_{ab}\rangle$	$\tilde{h}_{PP}(q^2)$
$\mathcal{M}_{\rm GT}^{AT_1} = \langle h_{AX}(q^2)(\boldsymbol{\sigma}_a \cdot \boldsymbol{\sigma}_b)\rangle$	$\tilde{h}_{AX}(q^2) = \frac{1}{(1+q^2/m_V^2)^2}\frac{1}{(1+q^2/m_A^2)^2}$
$\mathcal{M}_{\rm GT}^{\prime PT_1} = \langle \frac{\mathbf{q}^2}{m_p^2} h_{XP}(q^2)(\boldsymbol{\sigma}_a \cdot \boldsymbol{\sigma}_b)\rangle$	$\tilde{h}_{XP}(q^2) = \frac{1}{(1+q^2/m_V^2)^2}\frac{1}{(1+q^2/m_A^2)^2}\frac{1}{1+q^2/m_\pi^2}$
$\mathcal{M}_T^{\prime PT_1} = \langle \frac{\mathbf{q}^2}{m_p^2} h_{XP}(q^2) S_{ab}\rangle$	$\tilde{h}_{XP}(q^2)$
$\tilde{\mathcal{M}}_{\rm GT}^{AP'} = \langle \frac{\mathbf{Q}\cdot\mathbf{q}}{m_p^2} h_{AP}(q^2)(\boldsymbol{\sigma}_a \cdot \boldsymbol{\sigma}_b)\rangle \approx \mathcal{M}_{\rm GT}^{\prime AP}$	$\tilde{h}_{AP}(q^2)$
$\tilde{\mathcal{M}}_T^{AP'} = \langle \frac{\mathbf{Q}\cdot\mathbf{q}}{m_p^2} h_{AP}(q^2) S_{ab}\rangle \approx \mathcal{M}_T^{\prime AP}$	$\tilde{h}_{AP}(q^2)$
$\mathcal{M}_{\rm GT}^{\prime q_0 PP'} = \langle \frac{q_0\mathbf{q}^2}{m_p^3} h_{PP}(q^2)(\boldsymbol{\sigma}_a \cdot \boldsymbol{\sigma}_b)\rangle \approx 10^{-2}\mathcal{M}_{\rm GT}^{\prime P'P'}$	$\tilde{h}_{PP}(q^2)$
$\mathcal{M}_T^{\prime q_0 PP'} = \langle \frac{q_0\mathbf{q}^2}{m_p^3} h_{PP}(q^2) S_{ab}\rangle \approx 10^{-2}\mathcal{M}_T^{\prime P'P'}$	$\tilde{h}_{PP}(q^2)$

$$M_\nu = g_V^2\mathcal{M}_F - g_A^2\mathcal{M}_{\rm GT}^{AA} + \frac{g_A g_P}{6}(\mathcal{M}_{\rm GT}^{\prime AP} + \mathcal{M}_T^{\prime AP}) + \frac{(g_V+g_W)^2}{12}(-2\mathcal{M}_{\rm GT}^{\prime WW} + \mathcal{M}_T^{\prime WW}) - \frac{g_P^2}{48}(\mathcal{M}_{\rm GT}^{\prime\prime PP} + \mathcal{M}_T^{\prime\prime PP}). \quad (36)$$

Note that this is fully analogous to $\mathcal{M}_3$ in Eq. (32) in the case where the quark currents have the same chirality, but the crucial difference is that the NMEs in Eq. (36) are calculated with the appropriate neutrino potential in momentum space [29],

$$v(q) = \frac{2}{\pi}\frac{1}{q(q+\tilde{A})}. \quad (37)$$

Here, the neutrino mass has been neglected in comparison with the neutrino momentum $q \sim 100$ MeV, and $\tilde{A}$ is the closure energy, taken from Ref. [55] or estimated by the systematics, $\tilde{A} = 1.12\sqrt{A}$ MeV. This describes the long-range exchange of an essentially massless neutrino mediating $0\nu\beta\beta$ decay in this case. As noted earlier, the relative sign between the GT and T terms in Eq. (36) is different than in our previous papers [28–30,54] and other literature.

Our derivation of the NMEs performed within the phenomenological framework of the nucleon form factors can be compared with an alternative way which has been developed in the literature over recent years. It is based on chiral effective field theory [56], i.e., the effective theory describing interactions at low energy in terms of baryons, mesons, photons, and leptons [20,24,57,58]. In this approach the process of hadronization is replaced by a perturbative expansion in terms of q/Λ_χ reflecting the approximate chiral symmetry of QCD, where $\Lambda_\chi \simeq m_p \approx 1$ GeV is the chiral symmetry breaking scale. The chiral Lagrangian on which the corresponding calculation is

based should then incorporate all possible terms invariant under the chiral symmetry $SU(2)_L \times SU(2)_R$ in the same way as the corresponding quark-level operators. Each term then comes with a so-called low energy constant parametrizing the nonperturbative nature of QCD. Thus, the low energy constants play a role similar to that of the nuclear form factors arising in hadronization and their reliable determination, e.g., using lattice QCD input, is necessary to calculate the $0\nu\beta\beta$ decay rate in the chiral effective field theory (EFT) framework. The benefit of this approach is that one can avoid the factorization of the nucleon currents, which is a necessary approximation in the hadronization procedure.

C. Determination of NMEs in the IBM-2

In order to evaluate the NMEs we make use of the microscopic IBM-2 [59,60] which has the advantage that it can be used to all nuclei of interest. The interacting boson model has been one of the most successful models in reproducing collective features of the low-lying levels of medium as well as heavy nuclei, and is one of the few models that can be used consistently to all nuclei of interest. We have already studied different mechanisms systematically using the microscopic IBM-2 [28–30,54,61–63] and this study adds the short-range nonstandard mechanisms of double beta decay to the list.

The method of evaluation is discussed in detail in [28,30]. We use the interacting boson model with isospin restoration [30] in which isospin is restored by enforcing $M_F^{2\nu} = 0$ as in the quasi-particle random phase approximation calculations of [32,64]. Here we briefly mention the logic of the method, which is a mapping of the fermion operator H onto a boson space and its evaluation with bosonic wave functions. The mapping [65] can be done to leading order, next to leading order, etc.. In Ref. [28] it was shown, by explicit calculations, that next to leading order terms give, in general, negligible contributions, $\leq 1\%$. The matrix elements of the mapped operators are then evaluated with realistic wave functions, taken either from the literature, when available, or obtained from a fit to the observed energies and other properties [$B(E2)$ values, quadrupole moments, $B(M1)$ values, magnetic moments, etc.]. The values of parameters used in the current calculations are given in the Appendix A.

The single-particle and single-hole energies and strengths of interaction were evaluated and discussed in detail in Ref. [66] where the occupancies of the single particle levels were calculated in order to satisfy a twofold goal: to asses the goodness of the single particle energies and check the reliability of the used wave functions. Both tests are particularly important in the case of nuclei involved in double beta decay, as they affect the evaluation of the NMEs and then their reliability [67]. The energies of the single particle levels constitute a very important input for the calculation of the occupancies in the method used in Ref. [66]. In principle those energies can be considered as input parameters that can be fitted to reproduce the experimental occupancies. Instead of fitting, the single particle energies were extracted from experimental data on nuclei with a particle more or one particle less than a shell closure. These single particle energy sets were then used to calculate the occupancies of several nuclei of interest in double beta decay. Finally, the results were compared with other theoretical calculations and experimental occupancies, when available, and good correspondence was obtained. As part of the calculation single particle energies for several major shells were updated to values given in Appendix B.

Finally, an additional improvement is the introduction of short-range correlations in the nuclear structure calculation. These are of crucial importance for short-range nonstandard mechanisms and they can be taken into account by multiplying the potential $v(r)$ in coordinate space by a correlation function $f(r)$ squared. The most commonly used correlation function is the Jastrow function,

$$f_J(r) = 1 - ce^{-ar^2}(1 - br^2), \tag{38}$$

with $a = 1.1$ fm^{-2}, $b = 0.68$ fm^{-2}, and $c = 1$ for the phenomenological Miller-Spencer parametrization [68], and $a = 1.59$ fm^{-2}, $b = 1.45$ fm^{-2}, and $c = 0.92$ for the Argonne parametrization [69]. Since our formulation is in momentum space, we take short-range correlations into account by using the Fourier-Bessel transform of $f_J(r)$.

1. Numerical values of the NMEs

We present the numerical values all NMEs necessary to evaluate Eqs. (30)–(34) for the short-range mechanisms and for all relevant $0\nu\beta\beta$ decaying isotopes in Table II. They have been calculated within the IBM-2 as discussed above. This represents the first complete calculation of the NMEs needed for the description of short-range mechanisms of neutrinoless double beta decay. Note that the last four NMEs in Table I are not listed as they are derived from other NMEs as indicated therein. Likewise, Table III contains the NMEs for the standard light neutrino exchange mechanism, cf. Eq. (36). We remind the reader that in our convention where we calculate the NMEs using the reduced nucleon form factors $F_X(q^2)/g_X$, the NMEs in Tables II and III do not contain the form factor charges. They instead explicitly appear as coefficients in the expressions for $\mathcal{M}_1$ to $\mathcal{M}_5$ and for $\mathcal{M}_\nu$.

By specifically separating the value of g_A we allow for the possibility of a quenching of the axial-vector coupling. Even though quenching of g_A goes beyond the topic of this study, we would like to remind that it is well known from single beta decay and electron capture that g_A is renormalized in models of nuclei. Quenching of g_A in $2\nu\beta\beta$ decay, consistent with single-beta decay, has also been observed [29,30] (for a review see [70]). However, the question of whether or not g_A in $0\nu\beta\beta$ decay is

TABLE II. NMEs for short-range $0\nu\beta\beta$ decay mechanisms evaluated in the IBM-2 as described in the text and to be used in Eqs. (30)–(34). The values of the last four NMEs in Table I are not listed as they are derived from other NMEs as indicated therein.

Isotope	$\mathcal{M}_F$	$\mathcal{M}^{AA}_{\rm GT}$	$\mathcal{M}^{AT_1}_{\rm GT}$	$\mathcal{M}^{T_1T_1}_{\rm GT}$	$\mathcal{M}'^{WW}_{\rm GT}$	$\mathcal{M}'^{WW}_{T}$	$\mathcal{M}'^{AP}_{\rm GT}$	$\mathcal{M}'^{AP}_{T}$	$\mathcal{M}'^{PT_1}_{\rm GT}$	$\mathcal{M}'^{PT_1}_{T}$	$\mathcal{M}'^{P'P'}_{\rm GT}$	$\mathcal{M}'^{P'P'}_{T}$	$\mathcal{M}''^{PP}_{\rm GT}$	$\mathcal{M}''^{PP}_{T}$
^{76}Ge	−48.89	170.0	174.3	173.5	−2.945	−6.541	2.110	−1.310	2.255	−1.183	0.798	−0.271	0.028	−0.022
^{82}Se	−41.22	140.7	144.3	143.6	−2.456	−6.206	1.758	−1.249	1.878	−1.183	0.660	−0.259	0.024	−0.021
^{96}Zr	−35.31	124.3	128.5	128.8	−3.116	5.436	1.523	1.090	1.652	0.984	0.613	0.228	0.020	0.019
^{100}Mo	−51.96	181.9	188.1	188.6	−4.590	8.055	2.273	1.590	2.464	1.128	0.910	0.317	0.029	0.027
^{110}Pd	−43.52	151.2	156.5	157.0	−3.945	6.816	1.892	1.356	2.055	1.223	0.762	0.271	0.024	0.023
^{116}Cd	−32.45	110.5	114.6	115.2	−3.069	4.222	1.374	0.843	1.497	0.760	0.565	0.169	0.017	0.015
^{124}Sn	−33.19	104.2	106.7	106.1	−1.701	−3.655	1.321	−0.723	1.407	−0.651	0.489	−0.146	0.018	−0.012
^{128}Te	−41.82	131.7	134.9	134.1	−2.439	−4.519	1.667	−0.890	1.776	−1.433	0.617	−0.178	0.023	−0.015
^{130}Te	−38.05	119.7	122.6	121.9	−1.951	−4.105	1.514	−0.807	1.613	−0.726	0.561	−0.160	0.021	−0.014
^{134}Xe	−39.45	124.7	127.8	127.2	−2.111	−4.191	1.564	−0.823	1.669	−0.741	0.585	−0.163	0.021	−0.014
^{136}Xe	−29.83	94.18	96.56	96.09	−1.625	−3.158	1.177	−0.620	1.257	−0.558	0.442	−0.123	0.016	−0.011
^{148}Nd	−31.71	103.0	106.0	105.8	−2.145	2.557	1.346	0.510	1.445	0.460	0.508	0.104	0.018	0.009
^{150}Nd	−30.18	100.0	103.2	103.1	−2.230	2.955	1.292	0.581	1.392	0.523	0.497	0.116	0.017	0.010
^{154}Sm	−31.83	107.1	110.7	110.9	−2.618	3.397	1.356	0.668	1.467	0.601	0.536	0.135	0.018	0.012
^{160}Gd	−41.43	142.9	148.0	148.6	−3.808	5.231	1.776	1.023	1.931	0.920	0.722	0.205	0.023	0.018
^{198}Pt	−31.87	104.4	108.4	109.0	−2.992	3.172	1.334	0.626	1.454	0.564	0.546	0.119	0.017	0.011
^{232}Th	−44.04	154.2	159.7	160.3	−4.116	6.146	1.900	1.185	2.067	1.063	0.783	0.230	0.024	0.021
^{238}U	−52.48	183.1	189.7	190.5	−4.981	7.206	2.255	1.393	2.456	1.251	0.932	0.272	0.029	0.024

TABLE III. NMEs for the standard light neutrino exchange $0\nu\beta\beta$ decay mechanism evaluated in the IBM-2 as described in the text and to be used in Eq. (36).

Isotope	$\mathcal{M}_F$	$\mathcal{M}^{AA}_{\rm GT}$	$\mathcal{M}'^{AP}_{\rm GT}$	$\mathcal{M}'^{AP}_{T}$	$\mathcal{M}'^{WW}_{\rm GT}$	$\mathcal{M}'^{WW}_{T}$	$\mathcal{M}''^{PP}_{\rm GT}$	$\mathcal{M}''^{PP}_{T}$
^{76}Ge	−0.780	6.062	0.036	−0.010	0.089	−0.035	3.4×10^{-4}	-1.4×10^{-4}
^{82}Se	−0.667	4.928	0.030	−0.010	0.073	−0.034	4.1×10^{-4}	-1.3×10^{-4}
^{96}Zr	−0.361	4.317	0.027	0.009	0.065	0.032	3.1×10^{-4}	1.2×10^{-4}
^{100}Mo	−0.511	5.553	0.038	0.012	0.096	0.041	4.7×10^{-4}	1.6×10^{-4}
^{110}Pd	−0.425	4.432	0.032	0.009	0.080	0.036	3.9×10^{-4}	1.4×10^{-4}
^{116}Cd	−0.335	3.173	0.023	0.005	0.058	0.023	2.9×10^{-4}	8.7×10^{-5}
^{124}Sn	−0.572	3.370	0.021	−0.005	0.053	−0.018	2.5×10^{-4}	-7.5×10^{-5}
^{128}Te	−0.718	4.321	0.027	−0.005	0.067	−0.023	3.1×10^{-4}	-9.1×10^{-5}
^{130}Te	−0.651	3.894	0.024	−0.006	0.061	−0.021	2.8×10^{-4}	-8.3×10^{-5}
^{134}Xe	−0.686	4.211	0.026	−0.005	0.064	−0.023	3.0×10^{-4}	-8.3×10^{-5}
^{136}Xe	−0.522	3.203	0.019	−0.005	0.048	−0.016	2.2×10^{-4}	-6.3×10^{-5}
^{148}Nd	−0.363	2.517	0.020	0.005	0.053	0.014	2.6×10^{-4}	5.3×10^{-5}
^{150}Nd	−0.507	3.753	0.032	0.005	0.083	0.027	4.1×10^{-4}	9.7×10^{-5}
^{154}Sm	−0.340	2.984	0.022	0.005	0.056	0.018	2.7×10^{-4}	6.9×10^{-5}
^{160}Gd	−0.415	4.224	0.030	0.009	0.074	0.027	3.6×10^{-4}	1.1×10^{-4}
^{198}Pt	−0.329	2.270	0.021	0.005	0.054	0.014	2.7×10^{-4}	6.1×10^{-5}
^{232}Th	−0.444	4.169	0.032	0.009	0.079	0.032	3.9×10^{-4}	1.2×10^{-4}
^{238}U	−0.525	4.962	0.038	0.009	0.093	0.036	4.6×10^{-4}	1.4×10^{-4}

renormalized as much as in $2\nu\beta\beta$ is of much debate. This problem is currently being addressed both experimentally by employing single and double charge exchange reactions [71,72] and, theoretically, by using effective field theories to estimate the effect of non-nucleonic degrees of freedom [73]. Quenching of g_A arises from the omission of non-nucleonic degrees of freedom and from the limited model space in which the calculations are done. The former effect is not expected to be present in $0\nu\beta\beta$ decay since the average neutrino momentum is ∼100 MeV, while in $2\nu\beta\beta$ decay is of the order of 1–2 MeV. The latter effect instead appears both in $0\nu\beta\beta$ and $2\nu\beta\beta$ decays. This consideration suggests to use an effective value of $g_A^{\rm eff} = 1.0$, in between the free value $g_A = 1.269$ and the value observed in $2\nu\beta\beta$ decay, $g_A \sim 0.6$. We henceforth use this value.

2. Comparison with earlier results

From the NMEs in Tables II and III one can calculate the NMEs for the standard mass mechanism, $\mathcal{M}_\nu$ and heavy

TABLE IV. Comparison between the light neutrino exchange NMEs calculated in this work and those calculated in [30] using the quenched value $g_A = 1.0$ and the convention that $\mathcal{M}_\nu < 0$. The "old" F, GT, and T NMEs of Table I in [30] are combined in the NMEs $\mathcal{M}_\nu^{\rm old}$ and $\tilde{\mathcal{M}}_\nu^{\rm old}$ using a negative and positive sign of the tensor NME relative to that of the GT NME, respectively.

Isotope	$\mathcal{M}_F^{\rm old}$	$\mathcal{M}_{\rm GT}^{\rm old}$	$\mathcal{M}_T^{\rm old}$	$\mathcal{M}_\nu^{\rm old}$	$\tilde{\mathcal{M}}_\nu^{\rm old}$	$\mathcal{M}_F$	$\mathcal{M}_{\rm GT}$	$\mathcal{M}_T$	$\mathcal{M}_\nu$
^{76}Ge	−0.68	4.49	−0.23	−4.94	−5.40	−0.78	5.58	−0.28	−6.64
^{82}Se	−0.6	3.59	−0.23	−3.96	−4.42	−0.67	4.52	−0.27	−5.46
^{96}Zr	−0.33	2.51	0.11	−2.95	−2.73	−0.36	3.95	0.25	−4.07
^{100}Mo	−0.48	3.73	0.19	−4.40	−4.02	−0.51	5.08	0.32	−5.27
^{110}Pd	−0.40	3.59	0.21	−4.20	−3.78	−0.43	4.03	0.24	−4.21
^{116}Cd	−0.33	2.76	0.14	−3.23	−2.95	−0.34	2.89	0.12	−3.11
^{124}Sn	−0.57	2.96	−0.12	−3.41	−3.65	−0.57	3.10	−0.12	−3.79
^{128}Te	−0.72	3.80	−0.15	−4.37	−4.67	−0.72	3.97	−0.12	−4.80
^{130}Te	−0.65	3.43	−0.13	−3.95	−4.21	−0.65	3.59	−0.16	−4.40
^{134}Xe	−0.68	3.77	−0.15	−4.30	−4.60	−0.69	3.86	−0.12	−4.67
^{136}Xe	−0.52	2.83	−0.10	−3.25	−3.45	−0.52	2.96	−0.12	−3.60
^{148}Nd	−0.38	2.00	0.07	−2.45	−2.31	−0.36	2.28	0.12	−2.52
^{150}Nd	−0.39	2.33	0.10	−2.82	−2.62	−0.51	3.37	0.12	−3.76
^{154}Sm	−0.36	2.49	0.11	−2.96	−2.74	−0.34	2.71	0.12	−2.93
^{160}Gd	−0.45	3.64	0.17	−4.26	−3.92	−0.42	3.84	0.25	−4.00
^{198}Pt	−0.33	1.90	0.09	−2.32	−2.14	−0.33	2.02	0.12	−2.23
^{232}Th	−0.44	3.58	0.18	−4.20	−3.84	−0.44	3.76	0.25	−3.95
^{238}U	−0.53	4.27	0.21	−5.01	−4.59	−0.53	4.47	0.24	−4.75

neutrino exchange $\mathcal{M}_{\nu_h} = \mathcal{M}_3^{LL}$ to compare with earlier calculations. To this end, it is convenient to introduce the quantities

$$\mathcal{M}_{\rm GT} = \mathcal{M}_{\rm GT}^{AA} - \frac{g_P}{6g_A}\mathcal{M}_{\rm GT}^{\prime AP} + \frac{(g_V+g_W)^2}{6g_A^2}\mathcal{M}_{\rm GT}^{\prime WW} + \frac{g_P^2}{48g_A^2}\mathcal{M}_{\rm GT}^{\prime\prime PP}, \tag{39}$$

$$\mathcal{M}_T = \frac{g_P}{6g_A}\mathcal{M}_T^{\prime AP} + \frac{(g_V+g_W)^2}{12g_A^2}\mathcal{M}_T^{\prime WW} - \frac{g_P^2}{48g_A^2}\mathcal{M}_T^{\prime\prime PP}, \tag{40}$$

and write $\mathcal{M}_\nu$ as

$$\mathcal{M}_\nu = g_A^2\left[\left(\frac{g_V}{g_A}\right)^2\mathcal{M}_F - \mathcal{M}_{\rm GT} + \mathcal{M}_T\right], \tag{41}$$

and similarly for $\mathcal{M}_{\nu_h}$.

The values of the NMEs in the present work are compared with those in [30] in Table IV for light neutrino exchange and in Table V for heavy neutrino exchange. Comparing the old and new values of the F, GT, and T matrix elements one can see that the effect of improved single particle energies is sizeable in ^{76}Ge, ^{82}Se, ^{96}Zr, ^{150}Nd and small otherwise. The main difference between the calculation reported in [30] and the present one is in the sign of the tensor matrix element in Eq. (41). The present derivation gives a sign of the $\mathcal{M}_T$ term relative to that of $\mathcal{M}_F$, which is opposite to the one employed in Ref. [30]. This correction has little effect on the standard mass mechanism, for which $\mathcal{M}_T$ is small, but has considerable effect on the short-range mechanisms. Additionally, one can see that the matrix elements $\mathcal{M}_F$, $\mathcal{M}_{\rm GT}$, $\mathcal{M}_T$ for both light and heavy neutrino exchange are of the same order of magnitude in all elements with GT being the dominant term. This is due to the fact that the individual contributions given in Tables IV and V are all of the same order of magnitude and that the dominant term in $\mathcal{M}_3$ is $\mathcal{M}_{\rm GT}^{AA}$. The only difference comes from the sign of the tensor terms, $\mathcal{M}_T^{\prime AP}$, $\mathcal{M}_T^{\prime WW}$, $\mathcal{M}_T^{\prime\prime PP}$, which is different for the p-p and h-h case from the p-h and h-p case.

In Figs. 2 and 3 we, respectively, compare the compound NMEs $\mathcal{M}_\nu$ and $\mathcal{M}_{\nu_h}$ in the different calculations: present work (red circles), Ref. [30] (filled blue squares), and Ref. [30] with the correct sign for the tensor term (empty blue squares). This allows us to disentangle the effect of the new single particle energies from that induced by the sign of the tensor NME. As already mentioned, for light neutrino exchange (Fig. 2), the sign of the tensor term has relatively little impact, whereas the single particle energies lead to a sizeable increase of $\mathcal{M}_\nu$ in lighter isotopes. On the other hand, Fig. 3 demonstrates the strong effect of the sign of the tensor term in essentially all isotopes.

In comparison with calculations other than IBM-2 we note that our improved results for the standard mass mechanism are very similar to those in QRPA in all isotopes [31], but still differ from those of the shell model [74]. For the short-range mechanisms the obtained numbers are again similar to the QRPA in the case in which both

TABLE V. As Table IV, but comparing the heavy neutrino exchange NMEs calculated in this work and those given in Table IV of [30].

Isotope	$\mathcal{M}^{\text{old}}_{\nu_h,F}$	$\mathcal{M}^{\text{old}}_{\nu_h,GT}$	$\mathcal{M}^{\text{old}}_{\nu_h,T}$	$\mathcal{M}^{\text{old}}_{\nu_h}$	$\tilde{\mathcal{M}}^{\text{old}}_{\nu_h}$	$\mathcal{M}_{\nu_h,F}$	$\mathcal{M}_{\nu_h,GT}$	$\mathcal{M}_{\nu_h,T}$	$\mathcal{M}_{\nu_h}$
^{76}Ge	−42.8	104	−26.9	−120	−174	−48.9	115	−36.3	−200
^{82}Se	−37.1	87.2	−27.3	−97.0	−152	−41.2	94.7	−34.5	−171
^{96}Zr	−29.2	67.9	12.7	−110	−84.4	−35.3	80.2	30.2	−85.4
^{100}Mo	−46.8	111	24.2	−182	−134	−52.0	116	44.1	−124
^{110}Pd	−41.4	100	27.7	−169	−114	−43.5	96.2	37.5	−102
^{116}Cd	−31.2	73.9	16.9	−122	−88.2	−32.5	69.6	23.3	−78.8
^{124}Sn	−33.1	73.7	−14.9	−91.9	−122	−33.2	70.3	−20.0	−124
^{128}Te	−41.7	93.4	−18.3	−117	−153	−41.8	87.9	−24.7	−154
^{130}Te	−37.9	84.8	−16.6	−106	−139	−38.1	80.8	−22.4	−141
^{134}Xe	−39.3	86.6	−19.8	−106	−146	−39.5	84.1	−22.8	−146
^{136}Xe	−29.7	66.8	−12.7	−83.8	−109	−29.8	63.5	−17.2	−111
^{148}Nd	−32.7	72.8	9.60	−115	−95.9	−31.7	66.8	14.1	−84.4
^{150}Nd	−35.6	81.1	13.2	−130	−104	−30.2	64.5	16.1	−78.6
^{154}Sm	−33.7	78.1	13.8	−126	−98.0	−31.8	68.6	18.6	−81.9
^{160}Gd	−44.6	106	21.5	−172	−129	−41.4	90.8	28.5	−104
^{198}Pt	−31.9	71.4	12.8	−116	−90.5	−31.9	64.7	17.3	−79.3
^{232}Th	−44.0	107	24.4	−175	−127	−44.0	98.1	33.0	−109
^{238}U	−52.5	127	28.7	−208	−151	−52.5	116	38.8	−130

neutron and proton are particlelike (p-p) or holelike (h-h), while different in the case in which neutrons are holelike and protons are particlelike or vice versa (p-h and h-p). We also note that, although not discussed here, the main source of uncertainty for the matrix elements $\mathcal{M}_{\nu_h}$ is the parametrization of the short-range correlations. For example, for ^{76}Ge, QRPA reports [75] $\mathcal{M}_{\nu_h} = 32.6$ for Miller-Spencer, $\mathcal{M}_{\nu_h} = 233$ for Argonne, and $\mathcal{M}_{\nu_h} = 352$ for CD-Bonn parametrization, a factor of 10 difference. In the present paper we use the Argonne parametrization and obtain $\mathcal{M}_{\nu_h} = -200$ (see Table V) in reasonable agreement with the QRPA result, except for the overall sign in Eq. (41), which, as indicated above, is opposite to that of QRPA.

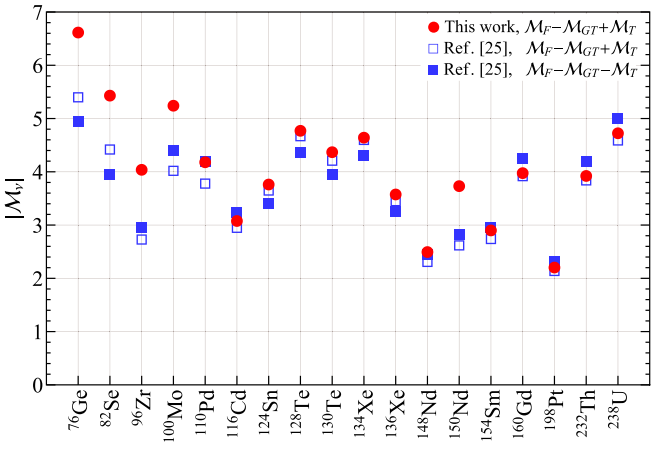

FIG. 2. Comparison between the light neutrino exchange IBM-2 NMEs $\mathcal{M}_\nu$ calculated in this work (red circles) and the ones calculated in [30] (solid blue squares), assuming the quenched value $g_A = 1.0$. We show also the old total NME $\tilde{\mathcal{M}}^{\text{old}}_\nu$ incorporating the (old) tensor part but with the correct sign (empty blue squares).

3. *Compound NMEs for short-range mechanisms*

Concluding our calculation of NMEs, in Table VI we summarize for clarity the numeric values of the compound NMEs $\mathcal{M}_1$ to $\mathcal{M}_5$ relevant for short-range $0\nu\beta\beta$ contributions, as defined in Eqs. (30)–(34). They are listed for all distinct combinations of quark chiralities and they are calculated using the quenched value $g_A = 1.0$. The values of light neutrino exchange NMEs $\mathcal{M}_\nu$ calculated in our approach are shown in the last column of Table IV.

We note that the NMEs $\mathcal{M}_1$ and $\mathcal{M}_5$ are generally enhanced due to the large pseudoscalar charges g_P and $g_{P'}$,

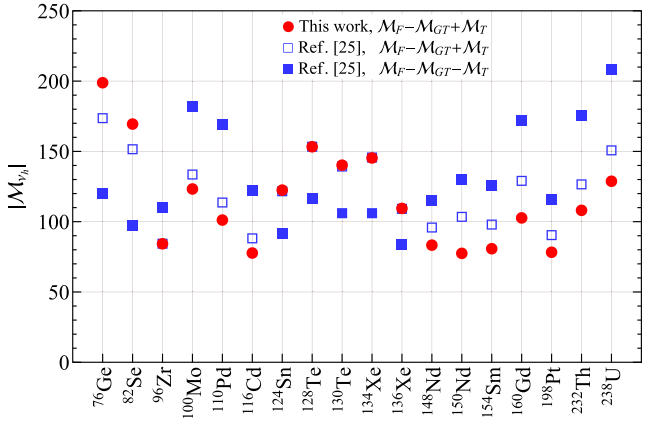

FIG. 3. As Fig. 2, but showing the comparison for the heavy-neutrino-exchange NME $\mathcal{M}_{\nu_h}$.

TABLE VI. Compound NMEs $\mathcal{M}_1$ to $\mathcal{M}_5$ for all distinct quark current chirality combinations, calculated using the quenched value $g_A = 1.0$.

Isotope	$\mathcal{M}_1^{XX}$	$\mathcal{M}_1^{XY}$	$\mathcal{M}_2^{XX}$	$\mathcal{M}_3^{XX}$	$\mathcal{M}_3^{XY}$	$\mathcal{M}_4^{XX}$	$\mathcal{M}_5^{XX}$	$\mathcal{M}_5^{XY}$
^{76}Ge	5300	−5400	−174	−200	99.8	−158	202	−301
^{82}Se	4030	−4110	−144	−171	83.3	−134	114	−199
^{96}Zr	8500	−8570	−129	−85.4	57.7	−88.6	832	−904
^{100}Mo	12400	−12500	−189	−124	83.9	−134	1230	−1340
^{110}Pd	10400	−10500	−157	−102	69.3	−107	1030	−1120
^{116}Cd	7420	−7480	−115	−78.8	52.0	−80.4	702	−768
^{124}Sn	3450	−3520	−106	−124	56.2	−95.3	157	−224
^{128}Te	4410	−4500	−134	−154	72.0	−130	205	−291
^{130}Te	4030	−4110	−122	−141	64.4	−109	187	−264
^{134}Xe	4240	−4320	−127	−146	67.6	−114	196	−277
^{136}Xe	3210	−3270	−96.1	−111	51.2	−86.0	147	−208
^{148}Nd	6180	−6240	−106	−84.4	46.2	−77.2	583	−648
^{150}Nd	6190	−6250	−103	−78.6	45.5	−74.2	591	−652
^{154}Sm	6780	−6840	−111	−81.9	50.0	−79.4	638	−703
^{160}Gd	9370	−9450	−149	−104	68.2	−105	886	−970
^{198}Pt	6720	−6780	−109	−79.3	49.3	−77.9	616	−681
^{232}Th	10200	−10300	−160	−109	74.0	−112	978	−1070
^{238}U	12200	−12300	−191	−130	88.1	−134	1160	−1260

though in $\mathcal{M}_5$ this is often compensated by the suppressed component NMEs. The enhancement is especially strong in isotopes with the same sign for $\mathcal{M}'^{P'P'}_{\mathrm{GT}}$ and $\mathcal{M}'^{P'P'}_{T}$ which arises from particle-particle versus particle-hole configurations of the nucleons. This, along with the large PSFs discussed below, makes ^{100}Mo an ideal isotope to probe the corresponding mechanisms from a theoretical point of view.

IV. LEPTONIC PHASE SPACE AND DECAY RATE

A. Leptonic matrix elements

Besides the NMEs, the calculation of the $0\nu\beta\beta$ decay rate requires the calculation of the so-called leptonic phase space factors. Here, we follow the numerical approach of Ref. [76]. Because of Pauli blocking of the inner states, the nucleons are expected to decay largely at the surface of the nucleus, which means that the electron wave function can be approximated by its value at the nuclear radius $r = R_A$.

Since we are interested only in $0^+ \to 0^+$ $0\nu\beta\beta$ transitions, nucleon operators of a certain parity must be combined with partial leptonic wave functions of the same parity. Specifically, the parity-even operators will be accompanied by $S_{1/2} - S_{1/2}$ and $P_{1/2} - P_{1/2}$ electron wave functions, while parity-odd ones will go together with the $S_{1/2} - P_{1/2}$ combination of wave functions. In this study we restrict ourselves only to the $S_{1/2} - S_{1/2}$ approximation, which allows us to drop the parity-odd nucleon operators from our calculation. The leptonic squared matrix elements for $S_{1/2} - S_{1/2}$ wave functions, summed over the electron spins s_1 and s_2, then read [27]

$$\sum_{s_1,s_2}(\bar{e}_1(1+\gamma_5)e_2^c)(\bar{e}_1(1\pm\gamma_5)e_2^c)^\dagger(1-P_{e_1e_2})/2 = f^{(0)}_{11\pm} + f^{(1)}_{11\pm}\hat{\mathbf{p}}_1\cdot\hat{\mathbf{p}}_2, \tag{42}$$

$$\sum_{s_1,s_2}(\bar{e}_1\gamma_\mu\gamma_5 e_2^c)(\bar{e}_1\gamma_\nu\gamma_5 e_2^c)^\dagger(1-P_{e_1e_2})/2 = \frac{1}{16}(f^{(0)}_{66} + f^{(1)}_{66}\hat{\mathbf{p}}_1\cdot\hat{\mathbf{p}}_2), \quad (\mu,\nu=0), \tag{43}$$

$$\sum_{s_1,s_2}(\bar{e}_1\gamma_\mu\gamma_5 e_2^c)(\bar{e}_1(1\pm\gamma_5)e_2^c)^\dagger(1-P_{e_1e_2})/2 = \mp\frac{1}{4}f^{(0)}_{16}, \quad (\mu=0), \tag{44}$$

where the scalar product between the asymptotic electron momentum vectors is parametrized as $\hat{\mathbf{p}}_1\cdot\hat{\mathbf{p}}_2 = \cos\theta$ with the opening angle $0 \le \theta \le \pi$. The term $(1 - P_{e_1e_2})$ indicates that the matrix element is antisymmetrized over the electrons. The result for Eq. (42) when both currents are left handed is the same as the one shown when both currents are right handed. Since we are interested only in $0^+ \to 0^+$ transitions in the $S_{1/2} - S_{1/2}$ approximation, we omit phase space factors corresponding to $\mu = j$ or $\nu = j$. Further, in Eqs. (42)–(44) we have used the quantities $f^{(0,1)}_{ij} \equiv f^{(0,1)}_{ij}(E_1, E_2)$ defined as

$$f^{(0)}_{11\pm} = \pm|f^{-1-1}|^2 \pm |f_{11}|^2 + |f^{-1}{}_1|^2 + |f_1{}^{-1}|^2,$$
$$f^{(1)}_{11\pm} = -2(f^{-1}{}_1 f_1{}^{-1} \pm f^{-1-1} f_{11}), \tag{45}$$

$$f^{(0)}_{66} = 16(|f^{-1-1}|^2 + |f_{11}|^2), \qquad f^{(1)}_{66} = 32 f^{-1-1} f_{11}, \tag{46}$$

$$f^{(0)}_{16} = 4(|f_{11}|^2 - |f^{-1-1}|^2), \qquad f^{(1)}_{16} = 0. \tag{47}$$

Here, the definitions in terms of electron wave functions $g_{-1}(E)$ and $f_1(E)$ evaluated at the nuclear surface apply, $f^{-1-1} = g_{-1}(E_1)g_{-1}(E_2)$, $f_{11} = f_1(E_1)f_1(E_2)$, $f^{-1}{}_1 = g_{-1}(E_1)f_1(E_2)$, $f_1{}^{-1} = f_1(E_1)g_{-1}(E_2)$. When compared to Refs. [11,17] our results agree but we also introduce additional factors $f^{(0,1)}_{11-}$, which appear as a result of the interference between the left- and right-handed scalar electron currents. In fact, these terms are not independent of the others as they can be expressed as $f^{(0,1)}_{11-} = f^{(0,1)}_{11+} - \frac{1}{8}f^{(0,1)}_{66\pm}$.

In determining the squared leptonic matrix elements, we numerically calculate the electron wave functions according to [76], taking into account the finite nuclear size and electron cloud screening corrections.

B. Differential decay distributions

The NMEs presented in the previous section and the squared leptonic matrix elements shown in Eqs. (42)–(44) can now be combined to calculate the rate of $0^+ \to 0^+\, 0\nu\beta\beta$ decay. The fully differential rate is expressed as [15–17]

$$\frac{d^2\Gamma}{dE_1 d\cos\theta} = Cw(E_1)(a(E_1) + b(E_1)\cos\theta), \quad (48)$$

with

$$C = \frac{G_F^4 \cos^4\theta_C m_e^2}{16\pi^5}, \qquad w(E_1) = E_1 E_2 p_1 p_2, \quad (49)$$

and where E_2, $p_1 = \sqrt{E_1^2 - m_e^2}$ and $p_2 = \sqrt{E_2^2 - m_e^2}$ are understood to be functions of E_1 due to overall energy conservation, $E_2 = Q_{\beta\beta} + 2m_e - E_1$. Here, $Q_{\beta\beta}$ is the so-called double beta decay Q value of the given isotope, i.e., the kinetic energy release of the electrons.

The coefficients $a(E_1)$ and $b(E_1)$ in Eq. (48) are, respectively, given by

$$\begin{aligned} a(E_1) = {} & f_{11+}^{(0)} \left| \sum_{I=1}^{3} \epsilon_I^L \mathcal{M}_I + \epsilon_\nu \mathcal{M}_\nu \right|^2 + f_{11+}^{(0)} \left| \sum_{I=1}^{3} \epsilon_I^R \mathcal{M}_I \right|^2 + \frac{1}{16} f_{66}^{(0)} \left| \sum_{I=4}^{5} \epsilon_I \mathcal{M}_I \right|^2 \\ & + f_{11-}^{(0)} \times 2\mathrm{Re}\left[\left(\sum_{I=1}^{3} \epsilon_I^L \mathcal{M}_I + \epsilon_\nu \mathcal{M}_\nu \right) \left(\sum_{I=1}^{3} \epsilon_I^R \mathcal{M}_I \right)^* \right] \\ & + \frac{1}{4} f_{16}^{(0)} \times 2\mathrm{Re}\left[\left(\sum_{I=1}^{3} \epsilon_I^L \mathcal{M}_I - \sum_{I=1}^{3} \epsilon_I^R \mathcal{M}_I + \epsilon_\nu \mathcal{M}_\nu \right) \left(\sum_{I=4}^{5} \epsilon_I \mathcal{M}_I \right)^* \right] \end{aligned} \quad (50)$$

and

$$b(E_1) = f_{11+}^{(1)} \left| \sum_{I=1}^{3} \epsilon_I^L \mathcal{M}_I + \epsilon_\nu \mathcal{M}_\nu \right|^2 + f_{11+}^{(1)} \left| \sum_{I=1}^{3} \epsilon_I^R \mathcal{M}_I \right|^2 + \frac{1}{16} f_{66}^{(1)} \left| \sum_{I=4}^{5} \epsilon_I \mathcal{M}_I \right|^2. \quad (51)$$

These expressions are valid under the presence of any combination of short-range mechanisms, with associated particle coefficients ϵ_I, and the standard light neutrino exchange where the coefficient ϵ_ν is defined by $\epsilon_\nu = m_{\beta\beta}/m_e$. Here, $m_{\beta\beta}$ is the usual effective $0\nu\beta\beta$ mass given in Eq. (8). The NMEs M_I and M_ν are defined in Eqs. (30)–(34) and (36), respectively, where the summations are over the different short-range current types $i = 1, \ldots, 5$ including their different chiralities, $I = (i, XYZ)$ with $X, Y, Z \in \{L, R\}$. A distinction is made between short-range mechanisms of type $i = 1, 2, 3$ for which the scalar current is left handed or right handed. This is indicated by ϵ_I^L and ϵ_I^R, respectively, where the sum is only over the corresponding terms. This distinction represents the interference behavior between terms of different electron chiralities. For example, the first term on the right-hand side of Eq. (50) describes the contributions of and the interference among the $i = 1, 2, 3$ short-range mechanisms ϵ_i^{XYL} with left-handed electron chiralities (but including all quark current chiralities) and that of the standard light neutrino exchange. Likewise the second term describes the contributions of $i = 1, 2, 3$ short-range mechanisms ϵ_I^R with right-handed electron chiralities including their cross interference, whereas the third term contains the interference between these two classes, $(\epsilon_{1,2,3}^L, \epsilon_\nu)$ with $\epsilon_{1,2,3}^R$. The other terms appearing in Eqs. (50) and (51) can be understood in a similar way where the electron-energy dependent factors $f_{ij}^{(0,1)} \equiv f_{ij}^{(0,1)}(E_1)$ describe the correctly associated squared lepton matrix elements as defined in Eqs. (45)–(47). Note that the interference term between short-range operators of type $i = 1, 2, 3$ and $i = 4, 5$ vanishes in $b(E_1)$ due to $f_{16}^{(1)} = 0$ in Eq. (47).

The fully differential decay rate Eq. (48) contains the complete kinematic information and integrating over the whole electron phase space will yield the total rate. Of experimental interest are the distribution over the single electron energy and the angular correlation. The single electron energy distribution is simply given by

$$\frac{d\Gamma}{dE_1} = 2Cw(E_1)a(E_1), \quad (52)$$

and the energy-dependent angular correlation is introduced as $\alpha(E_1) = b(E_1)/a(E_1)$. The latter has the property $-1 < \alpha(E_1) < +1$ and as it appears in front of the $\cos\theta$ term, it describes the likelihood for the electrons to be emitted back to back [$\alpha(E_1) \gtrsim -1$], collinearly [$\alpha(E_1) \lesssim +1$] or isotropically [$\alpha(E_1) \approx 0$]. Defining

$$\begin{aligned} A &= \int_{m_e}^{Q_{\beta\beta}+m_e} dE_1 w(E_1) a(E_1), \\ B &= \int_{m_e}^{Q_{\beta\beta}+m_e} dE_1 w(E_1) b(E_1), \end{aligned} \quad (53)$$

and their ratio $K = B/A$, the angular distribution reads

$$\frac{d\Gamma}{d\cos\theta} = \frac{\Gamma}{2}(1 + K\cos\theta). \tag{54}$$

With the given information we determine the single electron distribution $d\Gamma/dE_1$ and the angular correlation $\alpha(E_1)$ for the three relevant phase space factors that occur for short-range operators: $f^{(0,1)}_{11+}$ (for mechanisms $i = 1, 2, 3$ with a scalar electron current), $f^{(0,1)}_{66}$ (for mechanisms $i = 4, 5$ with an axial-vector electron current), $f^{(0)}_{16}$ (for interference between the two classes), and $f^{(0)}_{11-}$ (for interference between $i = 1, 2, 3$ of different lepton chirality). As already noted, $f^{(1)}_{16}$ vanishes, as does $f^{(1)}_{11-}$. The electron phase space distributions $f^{(0,1)}_{11+}$ also apply for the standard mass mechanism, calculated in the closure approximation.

The resulting single energy distribution and angular correlation were already presented in Ref. [27] for several isotopes, but in Fig. 4(left) we illustrate the normalized single energy distributions for ^{76}Ge as functions of the kinetic energy $E_1^{\rm kin} = E_1 - m_e$ of one of the electrons; i.e., the range is from zero up to $Q_{\beta\beta}$ value. As can be seen, the term $f^{(0)}_{11-}$ produces an energy distribution virtually indistinguishable from that of $f^{(0)}_{16}$. All mechanisms produce a hill-like shaped energy distribution and observing the single energy spectrum is not expected to help distinguish between the standard mass mechanism (corresponding to $f^{(0)}_{11+}$) and any of the short-range mechanisms. The angular correlation $\alpha(E_1^{\rm kin})$, shown in Fig. 4(right), can distinguish between different mechanisms, namely short-range mechanisms of type $i = 4, 5$ produce electrons that are emitted collinearly whereas for $i = 1, 2, 3$ and the standard mass mechanism, they are dominantly back to back. As mentioned, the factors $f^{(1)}_{16}$ and $f^{(1)}_{11-}$ vanish. There is therefore no change of the angular correlation due to interference and the angular correlation is an incoherent sum over contributions.

C. Total decay rate

Finally, we can integrate over the whole electron phase space to determine the total decay rate Γ and the decay half-life $T_{1/2}$,

$$\Gamma = \frac{\ln 2}{T_{1/2}} = 2C\int_{m_e}^{Q_{\beta\beta}+m_e} dE_1 w(E_1) a(E_1). \tag{55}$$

To facilitate calculation of the total rate under the presence of one or more mechanisms, we define the integrated PSFs [76]

$$G^{(0,1)}_{ij} = \frac{2C}{\ln 2}\frac{g^{(0,1)}_{ij}}{4R_A^2}\int_{m_e}^{Q_{\beta\beta}+m_e} dE_1 w(E_1) \times f^{(0,1)}_{ij}(E_1, Q_{\beta\beta} + 2m_e - E_1), \tag{56}$$

with $g^{(0,1)}_{11\pm} = 1$, $g^{(0,1)}_{66} = 1/16$, $g^{(0)}_{16} = 1/4$, $g^{(1)}_{16} = 0$. The factor $1/R_A^2$ has been introduced to conform with our convention where the NMEs are made dimensionless by multiplying with the nuclear radius R_A. The numerical values of the PSFs $G^{(0,1)}_{ij}$ are given in Table VII, in units of 10^{-15} yr^{-1}. As mentioned earlier, both $G^{(1)}_{16}$ and $G^{(1)}_{11-}$ vanish, corresponding to the absence of interference in the angular part $b(E_1)$.

With the above PSFs, the inverse $0\nu\beta\beta$ decay half-life can be written

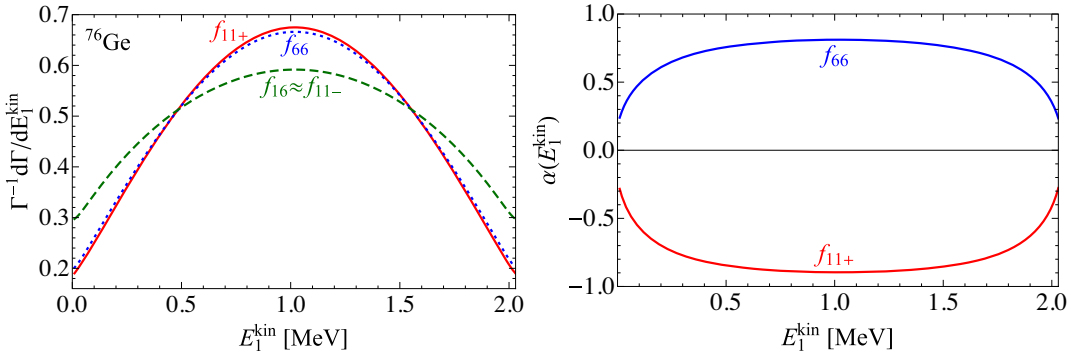

FIG. 4. Normalized single electron energy distributions $\Gamma^{-1}d\Gamma/dE_1^{\rm kin}$ (left) and angular correlation $\alpha(E_1^{\rm kin})$ (right) for ^{76}Ge as a function of the kinetic energy $E_1^{\rm kin} = E_1 - m_e$. Shown are the phase space factors for Eq. (50) in the former and for Eq. (51) in the latter.

$$T^{-1}_{1/2} = G^{(0)}_{11+}\left|\sum_{I=1}^{3}\epsilon^L_I\mathcal{M}_I + \epsilon_\nu\mathcal{M}_\nu\right|^2 + G^{(0)}_{11+}\left|\sum_{I=1}^{3}\epsilon^R_I\mathcal{M}_I\right|^2 + G^{(0)}_{66}\left|\sum_{I=4}^{5}\epsilon_I\mathcal{M}_I\right|^2 + G^{(0)}_{11-}\times 2\mathrm{Re}\left[\left(\sum_{I=1}^{3}\epsilon^L_I\mathcal{M}_I + \epsilon_\nu\mathcal{M}_\nu\right)\left(\sum_{I=1}^{3}\epsilon^R_I\mathcal{M}_I\right)^*\right] + G^{(0)}_{16}\times 2\mathrm{Re}\left[\left(\sum_{I=1}^{3}\epsilon^L_I\mathcal{M}_I - \sum_{I=1}^{3}\epsilon^R_I\mathcal{M}_I + \epsilon_\nu\mathcal{M}_\nu\right)\left(\sum_{I=4}^{5}\epsilon_I\mathcal{M}_I\right)^*\right]. \quad (57)$$

TABLE VII. PSFs in units of 10^{-15} yr^{-1} used in the calculation of the total decay rate for the standard light neutrino exchange and short-range mechanisms. The PSFs corresponding to $f^{(1)}_{11-}$ and $f^{(1)}_{16}$ vanish.

Isotope	$G^{(0)}_{11+}$	$G^{(0)}_{11-}$	$G^{(0)}_{66}$	$G^{(0)}_{16}$	$G^{(1)}_{11}$	$G^{(1)}_{66}$
			[10^{-15} yr^{-1}]			
^{76}Ge	2.360	−0.280	1.320	0.870	−1.954	0.977
^{82}Se	10.19	−0.712	5.450	2.925	−9.079	4.539
^{96}Zr	20.58	−1.190	10.88	5.403	−21.62	9.335
^{100}Mo	15.91	−1.053	8.482	4.456	−14.25	7.125
^{110}Pd	4.807	−0.541	2.674	1.730	−4.014	2.007
^{116}Cd	16.69	−1.187	8.938	4.843	−19.37	7.414
^{124}Sn	9.028	−0.843	4.935	2.976	−7.760	3.880
^{128}Te	0.585	−0.156	0.371	0.313	−0.390	0.195
^{130}Te	14.20	−1.142	7.672	4.367	−12.45	6.223
^{134}Xe	0.597	−0.164	0.380	0.323	−0.394	0.197
^{136}Xe	14.56	−1.197	7.876	4.524	−12.72	6.361
^{148}Nd	10.07	−1.084	5.579	3.548	−14.19	4.246
^{150}Nd	62.98	−3.125	33.05	15.44	−57.83	28.91
^{154}Sm	3.005	−0.539	1.772	1.338	−2.291	1.145
^{160}Gd	9.526	−1.129	5.321	3.506	−7.917	3.958
^{198}Pt	7.513	−1.305	4.409	3.278	−5.844	2.922
^{232}Th	13.87	−2.419	8.144	6.019	−10.92	5.457
^{238}U	33.45	−4.176	18.81	12.46	−28.02	14.01

Expressed in this way, the inverse half-life now only depends on the NMEs in Tables VI and IV (last column), the PSFs in Table VII and the coefficients ϵ_I, $\epsilon_\nu = m_{\beta\beta}/m_e$ encapsulating the particle physics aspects.

V. RESULTS

A. Bounds on the effective neutrino mass

With $\epsilon_\nu = m_{\beta\beta}/m_e$ and the other short-range ϵ_I set to zero, Eq. (57) simplifies to the well know formula for light neutrino exchange,

$$T^{-1}_{1/2} = \frac{|m_{\beta\beta}|^2}{m_e^2}G^{(0)}_{11+}|\mathcal{M}_\nu|^2. \quad (58)$$

Using the updated NME values for the light neutrino exchange mechanism shown in Table IV (last column) we can set new limits on the effective $0\nu\beta\beta$ mass $|m_{\beta\beta}|$. For isotopes with existing experimental bounds on the $0\nu\beta\beta$ decay rate, the resulting limits at 90% C.L. are summarized in Table VIII. As mentioned, the axial coupling is set to $g_A = 1.0$. Generally, the limits have improved compared to the previous analysis [30]. This is a consequence of the better experimental limits for ^{76}Ge, ^{82}Se, ^{130}Te, and ^{136}Xe as

TABLE VIII. Upper limits on the effective $0\nu\beta\beta$ mass $|m_{\beta\beta}|$ and the short-range ϵ_I couplings in units of 10^{-10} from current experimental bounds $T^{\mathrm{exp}}_{1/2}$ at 90% C.L., assuming a single contribution at a time and $g_A = 1.0$. The chiralities of the involved quark currents are specified: the label XX stands for the case when both chiralities are the same, $XX = RR, LL$, and XY applies if the chiralities are different, $XY = RL, LR$. The limit on ϵ_4 applies for all chirality combinations.

Isotope	$T^{\mathrm{exp}}_{1/2}$ [yr]		$\lvert m_{\beta\beta}\rvert$	$\lvert\epsilon^{XX}_1\rvert$	$\lvert\epsilon^{XY}_1\rvert$	$\lvert\epsilon^{XX}_2\rvert$	$\lvert\epsilon^{XX}_3\rvert$	$\lvert\epsilon^{XY}_3\rvert$	$\lvert\epsilon_4\rvert$	$\lvert\epsilon^{XX}_5\rvert$	$\lvert\epsilon^{XY}_5\rvert$
			[meV]				[10^{-10}]				
^{76}Ge	1.8×10^{26}	[9]	118	2.90	2.84	88.4	77.1	154	130	102	68.1
^{82}Se	2.4×10^{24}	[77]	599	15.9	15.5	445	375	768	654	764	440
^{96}Zr	9.2×10^{21}	[78]	9130	85.5	84.8	5640	8510	12600	11300	1200	1110
^{100}Mo	1.1×10^{24}	[79]	733	6.10	6.04	401	608	901	774	84.1	77.5
^{116}Cd	2.2×10^{23}	[80]	2720	22.3	22.1	1430	2090	3170	2800	321	294
^{128}Te	1.1×10^{23}	[81]	13300	283	277	9300	8080	17300	12100	7630	5390
^{130}Te	3.2×10^{25}	[82]	252	5.38	5.27	178	153	336	270	158	112
^{136}Xe	1.1×10^{26}	[83]	114	2.50	2.45	83.4	72.5	157	127	74	52.4
^{150}Nd	2.0×10^{22}	[84]	3830	45.5	45.1	2730	3590	6190	5240	659	596

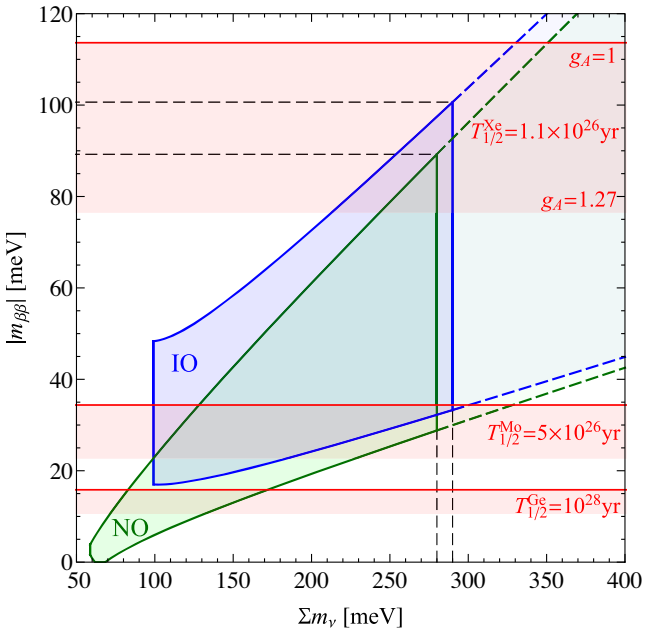

FIG. 5. Relation between the $0\nu\beta\beta$ mass $|m_{\beta\beta}|$ and the sum of neutrino masses Σm_ν for normally (NO) and inversely ordered (IO) neutrinos with the oscillation parameters fixed to the current best fit values. The dark shaded regions denote the parameter space allowed by the limits on Σm_ν at 95% C.L. from cosmological searches. The horizontal bars indicate the current upper limit on $|m_{\beta\beta}|$ and future sensitivities of $0\nu\beta\beta$ decay searches with an unquenched ($g_A = 1.27$, bottom edge) and quenched ($g_A = 1.0$, top edge) value of the axial coupling.

well as of the updated single particle energies in the NMEs for ^{76}Ge, ^{82}Se, ^{96}Zr, and ^{150}Nd.

In Fig. 5, we compare the existing limit and future sensitivities in a plot correlating the $0\nu\beta\beta$ mass $|m_{\beta\beta}|$ with the sum of neutrino masses $\Sigma m_\nu = m_{\nu_1} + m_{\nu_2} + m_{\nu_3}$ for the standard picture of three active neutrinos. The shaded regions indicate, as usual, the allowed parameter space for normally (NO) and inversely (IO) ordered neutrino spectra by varying over the Majorana CP phases, where we take the best fit values of the oscillation angles and mass-squared differences as given in [85]. Using our NMEs, the currently best limit is set by the KamLAND-Zen collaboration $T_{1/2}(^{136}\mathrm{Xe}) > 1.1 \times 10^{26}$ yr [83] resulting in $|m_{\beta\beta}| < 114$ meV at 90% C.L. for $g_A = 1.0$. The recent final result from GERDA with $T_{1/2}(^{76}\mathrm{Ge}) > 1.8 \times 10^{26}$ yr [9] corresponds to an essentially equal limit of $|m_{\beta\beta}| <$ 118 meV at 90% C.L. In Fig. 5 we also illustrate the corresponding limit assuming no quenching with $g_A =$ 1.27, giving $|m_{\beta\beta}| < 76$ meV. In addition to the current limit we also show two examples of prospective sensitivities $T_{1/2}(^{100}\mathrm{Mo}) = 5 \times 10^{26}$ yr expected at AMoRE-II [86] and $T_{1/2}(^{76}\mathrm{Ge}) = 10^{28}$ yr for LEGEND-1000 [87]. The latter will probe the full IO regime and a large chunk of the NO regime.

Neutrino masses are also probed by the cosmological effect of the relic neutrino background on the cosmic microwave background and the structure of the universe. Current observations are compatible with no effect arising from neutrino masses setting stringent limits on Σm_ν down to $\Sigma m_\nu < 150$ meV at 90% C.L. [88] The limit generally depends on the neutrino ordering due to different priors in the statistical analysis and it is affected by the choice of the astrophysical data. It can also be weakened if an underlying cosmological model other than the standard minimal ΛCDM is used. In Fig. 5 we show the most conservative limits arising from a choice of cosmological models surveyed in Ref. [88]. Namely, $\Sigma m_\nu < 280$ meV (NO) and $\Sigma m_\nu < 290$ meV (IO) at 95% C.L. arise in the ΛCDM with nonzero neutrino masses and a free scaling of the so-called weak lensing amplitude A_{lens} (ΛCDM+ $\Sigma m_\nu + A_{\mathrm{lens}}$). These limits correspond to $|m_{\beta\beta}| < 89$ meV (NO) and $|m_{\beta\beta}| < 101$ meV.

B. Bounds on effective short-range mechanisms

We can likewise assume that only a single short-range contribution is present by setting all other coefficients to zero and specifically assuming that the standard light neutrino contribution is negligible. Equation (57) then reduces to

$$T^{-1}_{1/2} = |\epsilon_I|^2 G_I |\mathcal{M}_I|^2, \tag{59}$$

with the PSF G_I and NME $\mathcal{M}_I$ depending on the type of contribution. From the current nonobservation of $0\nu\beta\beta$ decay we can then set upper limits on the effective ϵ_I couplings. These are also shown in Table VIII, using our calculated PSFs and NMEs with $g_A = 1.0$. Different chiralities of the quark currents in the operators lead to different bounds as indicated, where ϵ_i^{XX} denotes the case where the chiralities of the two quark currents are equal, $XX = LL, RR$, whereas ϵ_i^{XY} indicates that they are different, $XY = RL, LR$. For ϵ_2, the quark currents are required to be equal, cf. Eq. (6), and for ϵ_4, the bounds do not depend on the choice of the quark chiralities. Considering that a single ϵ_I contributes at a time, the limits do not depend on the lepton chirality as the corresponding PSFs are independent of it.

Numerically, the best limits for all ϵ_I are currently derived from the KamLAND-Zen constraint $T_{1/2}(^{136}\mathrm{Xe}) > 1.1 \times 10^{26}$ yr, except for ϵ_3^{XY} where the GERDA constraint is slightly better. In any case, the KamLAND-Zen and GERDA bounds result in essentially equally stringent limits in most of the cases, and they are of the order 10^{-10} to 10^{-8}. For ϵ_1 and ϵ_5, in addition to the improved experimental bounds, the limits are the most stringent due to enhanced values of the nucleon current charges, specifically the large value of the intrinsic pseudoscalar

TABLE IX. As Table VIII, but for the short-range couplings $c_I = \epsilon_I(m_W)$ in units of 10^{-10}, defined at the scale $m_W = 80.4$ GeV and omitting $|m_{\beta\beta}|$. Compared to Table VIII, the limits on c_4 depend on whether the quark currents have the same (XX) or opposite (XY) chirality.

Isotope	$T_{1/2}^{\rm exp}$ [yr]		$\lvert c_1^{XX}\rvert$	$\lvert c_1^{XY}\rvert$	$\lvert c_2^{XX}\rvert$	$\lvert c_3^{XX}\rvert$	$\lvert c_3^{XY}\rvert$ $[10^{-10}]$	$\lvert c_4^{XX}\rvert$	$\lvert c_4^{XY}\rvert$	$\lvert c_5^{XX}\rvert$	$\lvert c_5^{XY}\rvert$
^{76}Ge	1.8×10^{26}	[9]	1.42	0.948	611	101	177	286	185	50.3	22.9
^{82}Se	2.4×10^{24}	[77]	7.74	5.19	2630	494	882	1450	934	361	148
^{96}Zr	9.2×10^{21}	[78]	42.9	28.5	26900	11200	14500	17300	16100	616	372
^{100}Mo	1.1×10^{24}	[79]	3.06	2.03	1930	800	1040	1200	1110	43.1	26.1
^{116}Cd	2.2×10^{23}	[80]	11.2	7.40	7390	2760	3650	4470	4000	165	98.9
^{128}Te	1.1×10^{23}	[81]	139	92.6	76800	10600	19900	26400	17300	3820	1810
^{130}Te	3.2×10^{25}	[82]	2.64	1.76	1490	202	387	589	386	79.2	37.5
^{136}Xe	1.1×10^{26}	[83]	1.23	0.819	717	95.4	180	277	181	37.2	17.6
^{150}Nd	2.0×10^{22}	[84]	22.8	15.1	18200	4720	7120	8720	7490	337	201

charge $g_{P'}$, see Eq. (24). In case of ϵ_3 the sign of the tensor nuclear matrix elements also plays an important role.

The limits in Table VIII on the effective couplings apply at the QCD scale $\Lambda_{\rm QCD} \approx 1$ GeV. As described in [27] following [89,90] one can instead define the couplings at the electroweak scale $m_W = 80.4$ GeV and evolve them to $\Lambda_{\rm QCD}$, where the appropriate bound can be set employing the experimental limit on the $0\nu\beta\beta$ decay half-life. Because different operators mix radiatively, a single contribution at m_W may generally induce several contributions at $\Lambda_{\rm QCD}$. The limits obtained in this way can be compared more directly with constraints derived from collider experiments. The resulting bounds on the couplings $c_I = \epsilon_I(m_W)$ at m_W, including QCD running effects, are displayed in Table IX. Note that the limit on $|\epsilon_4|$ splits into two different values $|c_4^{XX}|$ and $|c_4^{XY}|$, since the different quark current chiralities affect the running. Numerically, the limits can be weaker or stronger than those at $\Lambda_{\rm QCD}$ due to the overlapping effect of the QCD corrections and the mixing of operators. The already stringent limits on ϵ_1^{XX} and ϵ_1^{XY} improve further at m_W and c_1^{XY} is the most strongly constrained coupling by KamLAND-Zen. On the other hand, the limit on c_2^{XX} is relatively much weaker than that on ϵ_2^{XX}. This is an effect of the renormalization group mixing with c_1^{XX} and partial cancellation with this induced term.

The effective short-range operator couplings can be interpreted in terms of effective New Physics operator scales Λ_I where we simply match

$$\frac{1}{\Lambda_I^5} = \frac{G_F^2 \cos^2\theta_C}{2m_p} c_I, \tag{60}$$

using the couplings c_I defined at the electroweak scale. In Fig. 6 we illustrate the current bounds and expected future sensitivities in ^{76}Ge (blue), ^{100}Mo (orange), and ^{136}Xe (green). The colored bars indicate the lower bound on the given operator scale where the darkest shade corresponds to the current limit and the two increasingly lighter shades represent expected future sensitivities. For the three isotopes, the setups are these: (i) $T_{1/2}(^{76}\text{Ge})/(10^{26}\ \text{yr}) = 1.8$ (GERDA [9], current), 10 (LEGEND-200 [87]), 100 (LEGEND-1000 [87]); (ii) $T_{1/2}(^{100}\text{Mo})/(10^{26}\ \text{yr}) = 0.011$ (NEMO-3 [79], current), 5 (AMoRE-II [86]), 10 (CUPID [91]); (iii) $T_{1/2}(^{136}\text{Xe})/(10^{26}\ \text{yr}) = 1.1$ (KamLAND-Zen-400 [83], current), 5 (KamLAND-Zen-800 [92]), 9.2 (nEXO [93]). As before, we assume only one short-range contribution to be present at m_W and we neglect any contribution from light neutrino exchange. As can be seen, the strong limits on c_1^{XX} and c_1^{XY} probe operator scales up to 18 TeV. The weakest limits, applying to $c_{2,3,4}$, still probe scales of order 4–6 TeV.

C. Interference between light neutrino exchange and short-range mechanisms

So far we have only considered one mechanism (operator) to be present at a given time, either the light neutrino exchange or one of the short-range operators. We now discuss the effect of two or more mechanisms operating at the same time. A large number of combinations are of course possible, but at least the standard light neutrino contribution is expected to be present at some level in any case. This is because any new physics scenario that generates a $\Delta L = 2$ short-range operator is also expected to generate Majorana neutrino masses at a level to explain neutrino oscillations. Therefore, it is reasonable to look into the interference of one of the nonstandard short-range mechanisms with the standard light neutrino exchange. We here discuss a few illustrative scenarios.

We first consider the interference with the operator associated with ϵ_3^{LLL}. As we have seen in Sec. II B 1, it is triggered by heavy sterile neutrinos. Under the presence of ϵ_ν and ϵ_3^{LLL}, Eq. (57) simplifies to

$$T_{1/2}^{-1} = G_{11+}^{(0)} \left| \frac{m_{\beta\beta}}{m_e} \mathcal{M}_\nu + \epsilon_3^{LLL} \mathcal{M}_3^{LL} \right|^2. \tag{61}$$

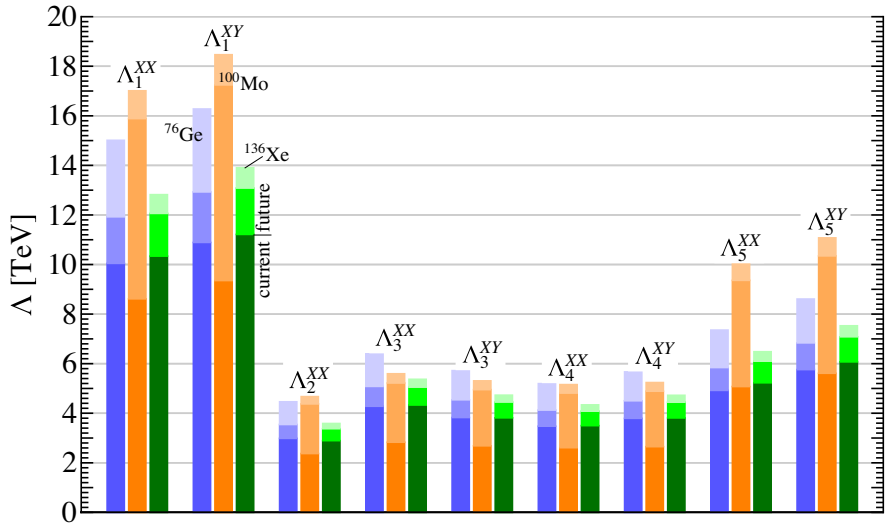

FIG. 6. Lower limits on the effective short-range operator scales Λ_I defined at m_W and assuming all other contributions are zero. The limits are from the current bounds (dark shade) and two future sensitivities (lighter shades) in ^{76}Ge at $(1.8, 10, 100) \times 10^{26}$ yr (left, blue), ^{100}Mo at $(0.011, 5, 10) \times 10^{26}$ yr (middle, orange) and ^{136}Xe at $(1.1, 5, 9.2) \times 10^{26}$ yr (right, green).

Because light neutrino exchange and the operator associated with ϵ_3^{LLL} have the same leptonic structure, the two contributions add coherently. The same behavior occurs for all operators of type $\epsilon_{1,2,3}$ with a left-handed leptonic current. Depending on the complex phases of the NMEs and the particle physics parameters $m_{\beta\beta}$, ϵ_3^{LLL}, the interference can be constructive or destructive. The NMEs are conventionally defined to be real with values given in Sec. III. In the given scenario, both NMEs are negative. We can choose $m_{\beta\beta}$ to be real and positive and the interference is described by the relative phase of ϵ_3^{LLL}. The largest effect then arises when ϵ_3^{LLL} is real and positive (constructive) or negative (destructive). Specifically, if $\epsilon_3^{LLL} = -|m_{\beta\beta}|/m_e(\mathcal{M}_\nu/\mathcal{M}_3^{LL})$, both contributions cancel each other.

The general constraints on the $(|m_{\beta\beta}|, \epsilon_3^{LLL})$ parameter space are depicted in Fig. 7 (left). As discussed, we take both $m_{\beta\beta}$ and ϵ_3^{LLL} to be relatively real with $m_{\beta\beta} > 0$ by convention. The light shaded areas are allowed given the current limits from $0\nu\beta\beta$ decays searches in ^{76}Ge and ^{136}Xe, whereas the dark shaded area denotes the sensitivity from future searches at $T_{1/2}(^{76}\text{Ge}) = 10^{28}$ yr. The combination of contributions in Eq. (61) leads to the linear relation between the variables and no independent limits can be set on them. From cosmological observations we can infer the upper limit $|m_{\beta\beta}| < 101$ meV, see Fig. 5, and neither $|m_{\beta\beta}|$ nor $|\epsilon_3^{LLL}|$ can be arbitrarily large given this additional constraint. Thus allowing a contribution $0 \le |m_{\beta\beta}| < 101$ meV from light neutrino exchange, ϵ_3^{LLL} is currently constrained to the interval $-137 \times 10^{-10} < \epsilon_3^{LLL} < 72.5 \times 10^{-10}$, compared to $|\epsilon_3^{LLL}| < 72.5 \times 10^{-10}$ in the case it is the only contribution. In Fig. 7(right), we show the equivalent plot in the $(|m_{\beta\beta}|, \Lambda_3^{LLL})$ parameter plane, where the effective operator scale is defined through $1/(\Lambda_3^{LLL})^5 = G_F^2 \cos^2\theta_C \epsilon_3^{LLL}/(2m_p)$. The current experimental constraints give $|\Lambda_3^{LLL}| \gtrsim 4.5$ TeV. If $m_{\beta\beta}$ is not restricted further independently, e.g., by inference from an improved measurement of Σm_ν, the future constraint $T_{1/2}(^{76}\text{Ge}) = 10^{28}$ yr will still allow $\Lambda_3^{LLL} \approx -4.8$ TeV due to destructive interference.

In the case of the interference between the standard light neutrino contribution with one operator of the type $\epsilon_{1,2,3}$ with a right-handed lepton current or of the type $\epsilon_{4,5}$, the overlap is suppressed by the interference between the different lepton currents involved. We here discuss the example ϵ_5^{RR} in which case Eq. (57) simplifies to

$$\begin{aligned} T_{1/2}^{-1} &= G_{11+}^{(0)}|\mathcal{M}_\nu|^2 \frac{|m_{\beta\beta}|^2}{m_e^2} + G_{66}^{(0)}|\mathcal{M}_5^{RR}|^2|\epsilon_5^{RR}|^2 \\ &\quad + 2G_{16}^{(0)}(\mathcal{M}_\nu\mathcal{M}_5^{RR})\text{Re}\left[\frac{m_{\beta\beta}}{m_e}\epsilon_5^{RR*}\right], \\ &= A|m_{\beta\beta}|^2 + B|\epsilon_5^{RR}|^2 - 2C|m_{\beta\beta}||\epsilon_5^{RR}|\cos(\alpha-\beta). \end{aligned} \tag{62}$$

Here, $A = G_{11+}^{(0)}|\mathcal{M}_\nu|^2/m_e^2$, $B = G_{66}^{(0)}|\mathcal{M}_5^{RR}|^2$, $C = G_{16}^{(0)}|\mathcal{M}_\nu|$ $|\mathcal{M}_5^{RR}|/m_e$ are positive coefficients (we consider the NMEs to be real with $\mathcal{M}_\nu$, $\mathcal{M}_5^{RR}$ having opposite signs, cf. Table VI), and α, β are the complex phases of $m_{\beta\beta}$, ϵ_5^{RR}, respectively. We again consider that the relative phase between $m_{\beta\beta}$ and ϵ_5^{RR} is $\alpha - \beta = 0, \pi$ in which case Eq. (62) is a quadratic function in $|m_{\beta\beta}|$ and ϵ_5^{RR} and for a

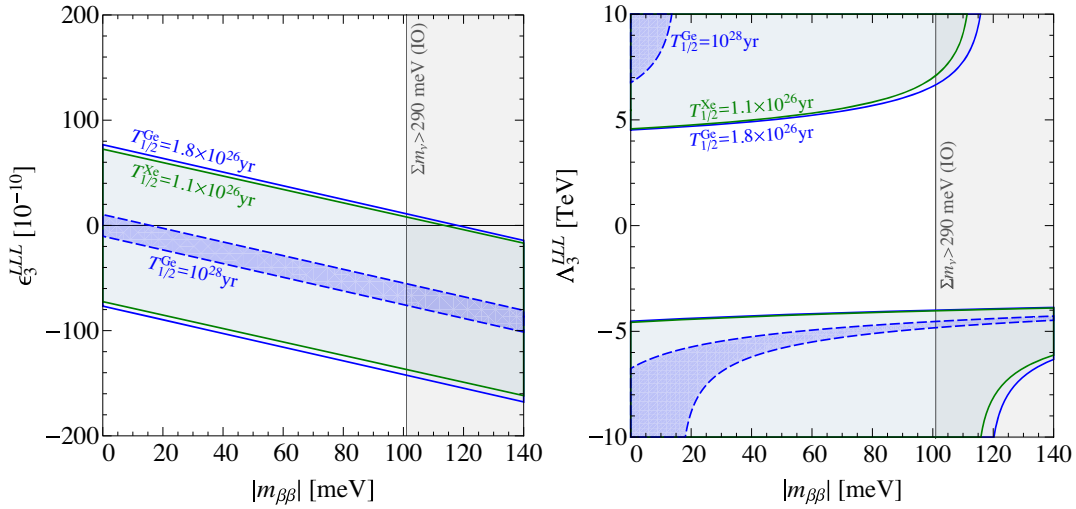

FIG. 7. Constraints on the effective $0\nu\beta\beta$ decay mass $|m_{\beta\beta}|$ and the short-range operator coupling ϵ_3^{LLL} (left) as well as the associated operator scale Λ_3^{LLL} (right). All other effective couplings are set to zero. The highlighted regions denote the allowed parameter space from the current limits $T_{1/2}(^{76}\mathrm{Ge}) > 1.8\times10^{26}$ yr (light blue) and $T_{1/2}(^{136}\mathrm{Xe}) > 1.1\times10^{26}$ yr (light green), as well as the future sensitivity $T_{1/2}(^{76}\mathrm{Ge}) = 10^{28}$ yr (dashed blue). The grey shaded area on the right is excluded assuming the bound on the sum of neutrino masses of $\Sigma m_\nu > 290$ meV from cosmological observations for an inverse neutrino mass ordering.

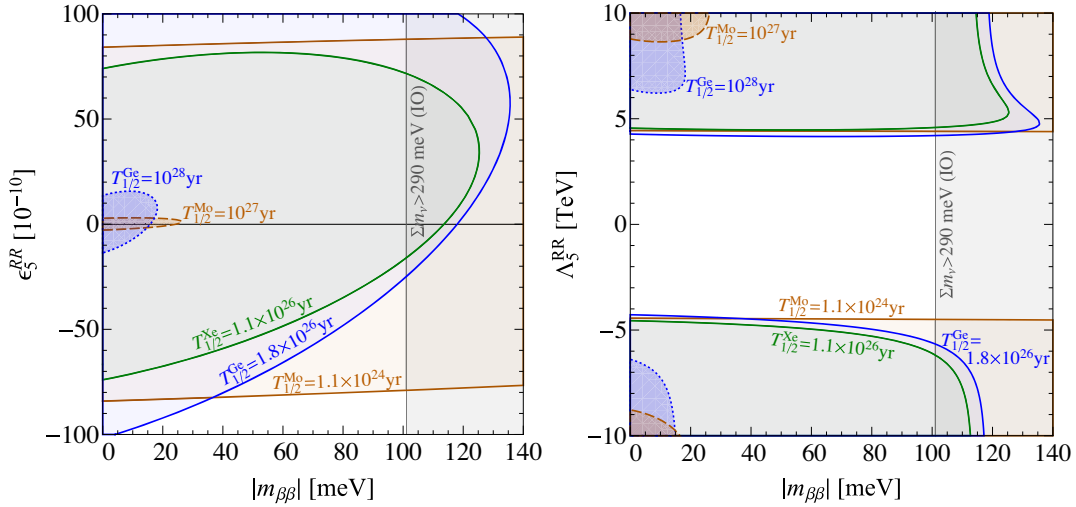

FIG. 8. As Fig. 7, but for the short-range operator coupling ϵ_5^{RR} and associated scale Λ_5^{RR}, also showing constraints from the current limit and future sensitivity in ^{100}Mo.

given value of $T_{1/2}^{-1}$ represent an ellipse. This is shown in Fig. 8(left) where the tilting is determined by the size of the PSF $G_{16}^{(0)}$ relative to $G_{11+}^{(0)}$ and $G_{66}^{(0)}$. The currently most stringent constraint is set in ^{136}Xe but the limit on ϵ_5^{RR} from ^{100}Mo is competitive despite the much weaker half-life limit. This is a consequence of enhanced NME $\mathcal{M}_5^{RR}$ in ^{100}Mo, see Table VI. Figure 8(right) shows the equivalent plot for the effective operator scale Λ_5^{RR}. As can be seen in Table VII, the PSFs $G_{16}^{(0)}$ applicable to all contributions of type $\epsilon_{4,5}$ are generally quite sizeable resulting in a comparatively strong interference. On the other hand, the PSF $G_{11-}^{(0)}$ regulates the interference with operators of type $\epsilon_{1,2,3}^R$ with right-handed lepton currents, see Eq. (57), which is suppressed by the electron mass compared to the beta decay $Q_{\beta\beta}$ value.

D. Constraints on new physics scenarios

The above constraints on the effective neutrino mass and short-range operator couplings can be interpreted in terms of the new physics scenarios introduced in Sec. II B.

1. Light and heavy sterile neutrinos

In the sterile neutrino case discussed in Sec. II B 1, we consider the simplified scenario where a single sterile neutrino of mass m_N with mixing V_{eN} to the electron neutrino contributes to $0\nu\beta\beta$ decay. The limiting cases where the sterile neutrino is much lighter and heavier than 100 MeV were discussed in Sec. II B 1. Currently, the most stringent limit in Table VIII on $0\nu\beta\beta$ decay contributions of heavy sterile neutrinos is set in ^{136}Xe,

$$\epsilon_3^{LLL} < 72.5 \times 10^{-10} \Rightarrow \left(\sum_{i=1}^{n_N} \frac{V_{eN_i}^2}{m_{N_i}}\right)^{-1} > 1.3 \times 10^8 \text{ GeV}, \tag{63}$$

assuming that the contributions from the light SM neutrinos are negligible.

To approximately incorporate the intermediate range $m_N \approx 100$ MeV as well, we use the interpolation [63,94]

$$T_{1/2}^{-1} = G_{11+}^{(0)} |\mathcal{M}_3^{LL}|^2 \left(\frac{m_p m_N}{\langle \mathbf{q}^2 \rangle + m_N^2}\right)^2 |V_{eN}|^4, \tag{64}$$

with the average momentum transfer $\langle \mathbf{q}^2 \rangle = m_p m_e |\mathcal{M}_3^{LL}/\mathcal{M}_\nu|$. In Fig. 9, we show the current limit and future sensitivity in the $(m_N, |V_{eN}|^2)$ parameter space. The region above the $0\nu\beta\beta$ bottom-most contours indicated are ruled out by the corresponding observation, assuming that the sterile neutrino is of a Majorana nature. We compare the $0\nu\beta\beta$ decay constraints with other searches for sterile neutrinos which are being pursued in neutrino oscillations, single beta decays, meson decays, at colliders and in electroweak precision measurements. The most recent searches are generally summarized in Ref. [95] and collider signatures are reviewed in Refs. [96,97]. The shaded area is excluded by current data and the dashed lines give examples of sensitivities in future searches. This includes the Tritium decay experiment KATRIN [98], searches for long-lived particles (LLP) (the shape is mainly determined by the planned DUNE [99], SHiP [100], and FCC-ee collider [101]) and high energy colliders FCC-hh [102], ILC [103], and CLIC [104,105]. As can be seen, future $0\nu\beta\beta$ decay searches at a level of $T_{1/2} \approx 10^{28}$ yr will be able to probe mixing strengths expected for light neutrino neutrino mass generation via the seesaw mechanism, $m_\nu = |V_{eN}|^2 m_N 0.01$ eV for $m_N \lesssim 100$ MeV. Likewise, $0\nu\beta\beta$ decay searches probe very heavy Majorana neutrinos with masses up to $m_N \approx 10^6$ GeV where electroweak precision measurements can otherwise set comparatively weak limits of order $|V_{eN}|^2 \lesssim 10^{-3}$.

We stress that this strong sensitivity of $0\nu\beta\beta$ decay searches applies to purely Majorana neutrinos, which are difficult to reconcile with the lightness of active neutrinos for $m_N \gtrsim 1$ GeV. For sterile neutrinos with such masses it is more natural that they form quasi-Dirac states where LNV is suppressed by a small mass splitting. In Fig. 9, we also show the sensitivity towards such a scenario where two Majorana neutrinos with a relative mass splitting of $\Delta m_N/m_N = 10^{-4}$ form a quasi-Dirac pair, partially cancelling their contributions to $0\nu\beta\beta$ decay. While the sensitivity is strongly reduced, $0\nu\beta\beta$ decay searches are

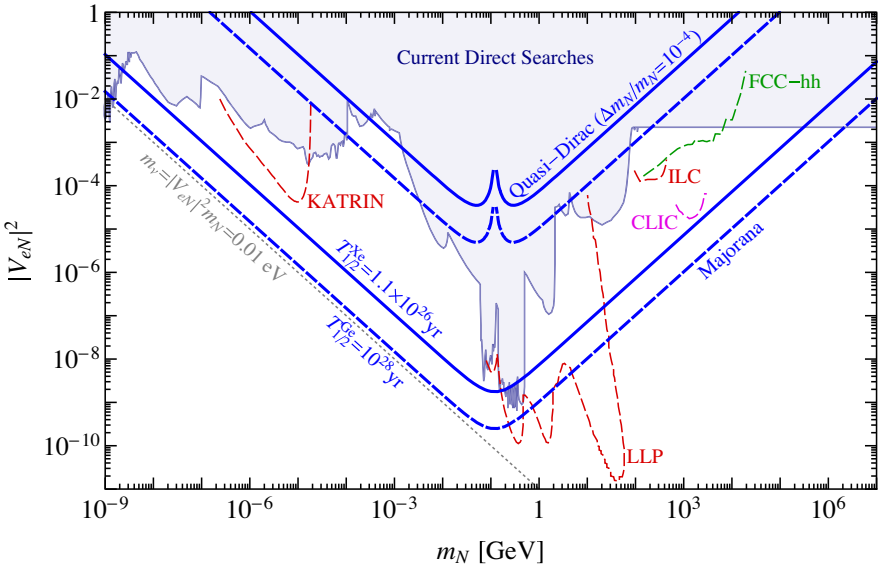

FIG. 9. Upper limit on the active-sterile neutrino mixing strength $|V_{eN}|^2$ as a function of the sterile neutrino mass m_N from current $0\nu\beta\beta$ decay searches (solid curves) and at future sensitivities with $T_{1/2} = 10^{28}$ yr (dashed curves). The sterile neutrino is assumed to be of Majorana or quasi-Dirac nature as indicated and contributions from light neutrinos are neglected. The blue shaded area is excluded by current data from neutrino oscillations, beta decays, meson decays, colliders, and electroweak precision measurements. The dashed contours indicate the estimated future sensitivity in Tritium decays (KATRIN), long-lived particle (LLP) searches and at colliders (FCC-hh, ILC, CLIC). The diagonal line gives the seesaw relation of light neutrino mass generation, $m_\nu = |V_{eN}|^2 m_N = 0.01$ eV.

still competitive at this level for $m_N \approx 1$ MeV and $m_N \approx 100$ GeV.

2. Left-right symmetry

In Fig. 10, we show the limits from $0\nu\beta\beta$ decay searches on the right-handed W_R boson mass m_{W_R} and the heavy neutrino mass m_N in the LRSM introduced in Sec. II B 2. Here, we consider a simplified scenario with one lepton generation, i.e., a single heavy neutrino N and $U^R_{e1} = 1$. We also choose the so-called manifest left-right symmetric case with $g_R = g$, $\cos\theta^R_C = \cos\theta_C$ and take $m_{\Delta^{--}_R} = m_{W_R}$ for the mass of the doubly charged triplet Higgs. The solid and dashed $0\nu\beta\beta$ curves give the lower limit on m_{W_R} where we additionally neglect the W boson mixing, $\sin\theta^W_{\rm LR} = 0$, thus ϵ^{RRR}_3 is the only contribution. The rise of the $0\nu\beta\beta$ curves to the right of $m_N \approx 10^3$ GeV in Fig. 10 results from the doubly charged Higgs contribution in Eq. (15) increasing linearly with m_N. Note, though, that too large values of m_N, compared to m_{W_R}, are not natural as they would require nonperturbative Yukawa couplings with the triplet Higgs.

The $0\nu\beta\beta$ decay limits are compared with the direct limits from the LHC and the future SHiP experiment. The current LHC limits arise from dijet, $e + E_{\rm miss}$ [106] and $eejj$ signatures [107]. The future LHC limits are estimated for 300 fb^{-1} of luminosity and are taken from [106]. The dijet and $e + E_{\rm miss}$ signatures are largely independent of the heavy neutrino mass in the applicable kinematic regimes and are sensitive to $m_{W_R} \approx 4$–7 TeV. On the other hand, the SHiP experiment would probe heavy neutrinos produced mainly in D meson decays and the strong sensitivity around $m_N \approx 1$ GeV shown is taken from Ref. [108]. As can be seen, $0\nu\beta\beta$ decay searches are especially sensitive for $m_N \lesssim 20$ GeV. Note that we only consider heavy neutrino masses as light as $m_N = 100$ MeV where the short-range contribution assumption is reasonable. For $m_N \approx 100$ MeV we incorporate the approximation in Eq. (64); masses around and below this scale can be incorporated using an analysis of the relevant dim-7 operators [18–20,109] and by including the mass dependence of the neutrino potential [63,94,110].

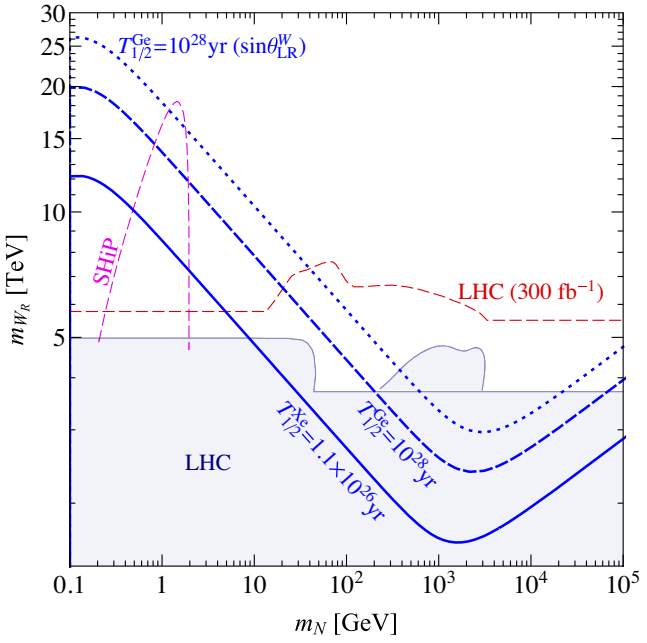

FIG. 10. Lower limit on the right-handed W_R boson mass m_{W_R} as a function of the right-handed neutrino mass m_N from current $0\nu\beta\beta$ decay searches (solid curve) and the corresponding future sensitivities with $T_{1/2}(^{76}{\rm Ge}) = 10^{28}$ yr (dashed curve) in the LRSM with negligible W boson mixing. The dotted curve indicates the future sensitivity on the scenario where the W boson mixing is $\sin\theta^W_{LR} = m^2_W/m^2_{W_R}$. The blue shaded area is excluded by current data from the LHC and the dashed contours indicate the estimated future sensitivity at the LHC with 300 fb^{-1} and at SHiP.

Both the LHC and SHiP limits were derived assuming negligible W boson mixing; those based on the lifetime of the heavy neutrino will be affected and need to be reassessed. We nevertheless also include the sensitivity of future $0\nu\beta\beta$ decay searches for $\sin\theta^W_{\rm LR} = m^2_W/m^2_{W_R}$, i.e., the generically maximal value expected, where all three operators ϵ^{RRR}_3, ϵ^{LLR}_3, ϵ^{LRR}_3 contribute. Future searches are then expected to be sensitive up to $m_{W_R} \approx 26$ TeV.

3. R-parity violating supersymmetry

Assuming gluino dominance, R-parity violating supersymmetry will induce the contributions in Eq. (18). Neglecting any other contributions, including those from light neutrinos, Eq. (57) simplifies to

$$T^{-1}_{1/2} = G^{(0)}_{11+}(1.95\mathcal{M}^{RR}_1 - 2.88\mathcal{M}^{RR}_2)^2 \times \left(\frac{8\pi\alpha_s\lambda'^2_{111}}{9\cos^2\theta_C}\frac{G_F^{-2}}{m^4_{\tilde q}}\frac{m_p}{m_{\tilde g}}\right)^2, \quad (65)$$

where the numerical factors in front of the NMEs take into account the effect of QCD running; i.e., we here interpret the coupling strength λ'_{111} at m_W. Using the current KamLAND-Zen bound $T_{1/2}(^{136}{\rm Xe}) > 1.1 \times 10^{26}$ yr, this can be translated into an upper limit on λ'_{111},

$$\lambda'_{111} < 7.0 \times 10^{-3}\left(\frac{m_{\tilde q}}{1\ {\rm TeV}}\right)^2\left(\frac{m_{\tilde g}}{1\ {\rm TeV}}\right)^{1/2}. \quad (66)$$

This compares to the limit $\lambda'_{111} < 7.2 \times 10^{-3}$ in [111][1] for the same squark and gluino masses and the above KamLAND-Zen bound. Somewhat surprisingly, the limits are thus of a very similar size; whereas, in our case, the strong sensitivity is predominantly due to the enhanced

[1]Reference [111] contains updated experimental constraints and includes the effects of QCD running to the scale 1 TeV compared to [46].

value of the NME $\mathcal{M}_1^{RR}$ resulting from the large pseudoscalar form factor in Eq. (24), in Ref. [111] it is an effect of the QCD running and operator mixing.

If $0\nu\beta\beta$ decay is not observed in future experiments with a sensitivity approaching $T_{1/2}(^{100}\mathrm{Mo}) = 10^{27}$ yr, the limit will improve to

$$\lambda'_{111} < 2.0 \times 10^{-3} \left(\frac{m_{\tilde{q}}}{1\ \mathrm{TeV}}\right)^2 \left(\frac{m_{\tilde{g}}}{1\ \mathrm{TeV}}\right)^{1/2}. \quad (67)$$

This is mainly a result of the strong sensitivity to ϵ_1^{RR} especially in ^{100}Mo, see Sec. V B. As mentioned, the derived limit is based on the assumption of gluino dominance. It will be important to reevaluate the impact of $0\nu\beta\beta$ decay searches on the R-parity violating supersymmetry in light of the new results and the current constraints from direct searches for supersymmetric particles.

VI. SUMMARY AND CONCLUSION

Signatures of total lepton number violation are crucial if we want to understand the origin of neutrino masses, which constitute a key open issue in particle physics. Neutrinoless double beta decay has so far been the only practical means to probe light Majorana neutrino masses at scales indicated by neutrino oscillations. In addition it is sensitive to new physics contributions from exotic particles and interactions coupling to first-generation quarks and electrons. Within an EFT framework, $0\nu\beta\beta$ decay searches strongly constrain contributions of that form. In this work we have concentrated on short-range contributions which result from integrating out exotic particles much heavier than the energy scale $m_F \approx 100$ MeV of double beta decay, leading to effective dimension-nine operators of the form $\Lambda^{-5}\bar{u}\,\bar{u}\,dd\bar{e}\,\bar{e}$. In addition, we update calculations for the standard light neutrino exchange mechanism to analyze the interplay with short-range contributions.

We have presented a first complete numerical evaluation of the NMEs needed for the description of short-range nonstandard mechanisms of $0\nu\beta\beta$ decay. The calculation is performed within the framework of IBM-2 with restoration of the isospin properties of the Fermi transition operator. We also use updated single particle energies extracted from experimental data on nuclei with one nucleon removed or added from shell closure. We include additional NMEs that become important when the latest values of the nucleon form factors are taken into account. However, the main difference to previous calculations is in the sign of the tensor NMEs; the present derivation gives a sign of the tensor term $\mathcal{M}_T$, which is opposite to that in, e.g., [30]. This change has little effect on the standard mechanism, for which $\mathcal{M}_T$ is small $\approx 1\%$, but it is sizeable for short-range mechanisms.

As noted, we have performed our calculation in the phenomenological framework of the interacting boson model, using nucleon currents in the impulse approximation including higher-order terms in the nucleon momentum transfer determined in [27]. We model pion-mediated modes via enhanced pseudoscalar nucleon form factors informed by partially conserved axial-vector current and lattice QCD calculations. In our numerical results we consider a possible quenching of the axial-vector coupling by choosing $g_A = 1.0$ compared to the unquenched value $g_A = 1.27$. We follow this classical approach in contrast to *ab initio* methods based on chiral EFT interactions [56]. Such formulations promise the determination of NMEs with controllable errors, e.g., may address part of the quenching problem [112]. Calculations of the standard light neutrino exchange NME $\mathcal{M}_\nu$ following this approach have become possible for the lightest double beta decay isotopes ^{48}Ca [113–115], ^{76}Ge, and ^{82}Se [114], indicating noticeably smaller values than those from phenomenological models such as IBM-2, see [116] for a recent review. If confirmed, this will require an understanding for such a deviation as well further studies to apply *ab initio* methods to heavier nuclei. NMEs should ideally be verified experimentally by employing single and double charge exchange reactions [71,72]. Chiral EFT techniques have been used to reveal a potentially sizeable short-range contribution in standard light neutrino exchange [57] and to calculate exotic contributions [20,24].

In addition to the NMEs calculated in our approach we also present the full set of leptonic PSFs for all relevant isotopes, determined numerically including effects from the finite nuclear size and electron cloud screening corrections. This allows us to set updated limits on the effective couplings of all possible short-range operators contributing to $0\nu\beta\beta$ decay. Considering one operator at a time, the current limits correspond to operator scales ranging between 3 to 10 TeV, where the strongest sensitivity is achieved for operators enhanced by pion-mediated corrections, in agreement with previous analyses [24,117–119], in our case arising from enhanced pseudoscalar form factors. We further illustrate the interplay between different contributions by considering the interference between the standard light neutrino exchange with one short-range contribution ϵ_I thus setting constraints on the combined parameter space $(m_{\beta\beta}, \epsilon_I)$. Finally, we apply the effective operator framework to three example new physics scenarios, namely the SM with sterile neutrinos, left-right symmetry, and R-parity violating supersymmetry. Here, we set updated constraints on simplified parameter spaces and compare them with limits coming from other searches.

Searches for lepton number violating signatures, with $0\nu\beta\beta$ decay as the most prominent example, are crucial for our understanding of neutrinos and physics beyond the SM in general. Given that no clear sign of new physics has been seen so far, short-range operators as those considered in this work provide a model-agnostic means to probe the presence of lepton number violating physics. Due to the strong suppression—the $0\nu\beta\beta$ decay rate scales as $\propto \Lambda^{-10}$—future experimental advances increasing the sensitivity by up to

two orders of magnitude to half-lives $T_{1/2}^{0\nu\beta\beta} \approx 10^{27-28}$ yr will only result in modest improvements in constraining Λ, see Fig. 6. Detailed analyses such as our work and [24] are still important as these operator scales $\Lambda \approx 4$–18 TeV are in a regime relevant for the LHC and potential future colliders. If an exotic short-range contribution were to be observed, it would indicate that light neutrino masses have their origin around the TeV scale. It would also have profound consequences on possible explanations of the matter-antimatter asymmetry of the Universe, with the observation of nonstandard $0\nu\beta\beta$ decay contributions disfavoring baryogenesis mechanisms operating above the electroweak scale [26,120].

ACKNOWLEDGMENTS

The authors would like to thank Jose Barea for providing the code to calculate standard mechanisms of double beta decay in IBM-2 and Patrick Bolton for sharing the direct sterile neutrino search limits and sensitivities. The authors would also like to thank Martin Hirsch for a careful reading of the manuscript and useful discussions. This work was supported in part by the U.S. Department of Energy (Grant No. DE-FG-02-91ER-40608) and the UK Royal Society International Exchange program. The work of J. K. was supported by the Academy of Finland (Grants No. 314733 and No. 320062). L. G. and F. F. D. acknowledge support from the UK Science and Technology Facilities Council (STFC) via a Consolidated Grant (Reference ST/P00072X/1).

APPENDIX A: PARAMETERS OF THE IBM-2 HAMILTONIAN

A detailed description of the IBM-2 Hamiltonian is given in [60,121]. For most nuclei, the Hamiltonian parameters are taken from the literature [122–135]. The new calculations are done using the program NPBOS [121].

TABLE X. Hamiltonian parameters employed in the IBM-2 calculation of the wave functions along with their references.

Nucleus	ϵ_{d_ν}	ϵ_{d_π}	κ	χ_ν	χ_π	ξ_1	ξ_2	ξ_3	$c_\nu^{(0)}$	$c_\nu^{(2)}$	$c_\nu^{(4)}$	$c_\pi^{(0)}$	$c_\pi^{(2)}$	$c_\pi^{(4)}$	$\omega_{\nu\nu}$	$\omega_{\pi\pi}$	$\omega_{\nu\pi}$	w_ν	y_ν
^{76}Ge [122]	1.20	1.20	−0.21	1.00	−1.20	−0.05	0.10	−0.05											
^{76}Se [123]	0.96	0.96	−0.16	0.50	−0.90			−0.10											
^{82}Se [123]	1.00	1.00	−0.28	1.14	−0.90			−0.10											
^{82}Kr [124]	1.15	1.15	−0.19	0.93	−1.13	−0.10		−0.10											
^{96}Zr[a]	1.00	1.00	−0.20	−2.20	0.65										0.17	0.17	0.33		
^{96}Mo [125]	0.73	1.10	−0.09	−1.20	0.40	−0.10	0.10	−0.10	−0.50	0.10									
^{100}Mo [125]	0.55	1.00	−0.06	−1.20	0.40	−0.10	0.10	−0.10	−0.60	0.20	0.10								
^{100}Ru [126]	0.89	0.89	−0.18	−1.00	0.40				0.60	0.09	−0.13								
^{110}Pd [127]	0.78	0.60	−0.13	0.00	−0.30	0.20	0.04	0.00	−0.26	−0.29	−0.30	−0.26	−0.29	−0.03					
^{110}Cd [128]	0.92	0.92	−0.15	−1.10	−0.80	1.10	0.109	1.10	0.07	−0.17	0.16								
^{116}Cd [129]	0.85	0.85	−0.27	−0.58	0.00	−0.18	0.24	−0.18	−0.15	−0.06									
^{116}Sn [130]	1.32								−0.50	−0.22	−0.07							−0.06	0.04
^{124}Sn[b]	1.10								−0.30	−0.16	−0.20							0.30	0.02
^{124}Te [129]	0.82	0.82	−0.15	0.00	−1.20	−0.18	0.24	−0.18	0.10										
^{128}Te [129]	0.93	0.93	−0.17	0.50	−1.20	−0.18	0.24	−0.18	0.30	0.22									
^{128}Xe [131]	0.70	0.70	−0.17	0.33	−0.80	−0.18	0.24	−0.18	0.30										
^{130}Te [129]	1.05	1.05	−0.20	0.90	−1.20	−0.18	0.24	−0.18	0.30	0.22									
^{130}Xe [131]	0.76	0.76	−0.19	0.50	−0.80	−0.18	0.24	−0.18	0.30	0.22									
^{136}Xe[b]		1.31										−0.04	0.01	−0.02					
^{136}Ba [131]	1.03	1.03	−0.23	1.00	−0.90	−0.18	0.24	−0.18	0.30	0.10									
^{148}Nd [132]	0.70	0.70	−0.10	−0.80	−1.20	−0.12	0.24	0.90				0.40	0.20						
^{148}Sm [132]	0.95	0.95	−0.12	0.00	−1.30	−0.12	0.24	0.90					0.05						
^{150}Nd [132]	0.47	0.47	−0.07	−1.00	−1.20	−0.12	0.24	0.90				0.40	0.20						
^{150}Sm [132]	0.70	0.70	−0.08	−0.80	−1.30	−0.12	0.24	0.90					0.05						
^{154}Sm [132]	0.43	0.43	−0.08	−1.10	−1.30	−0.12	0.24	0.90					0.05						
^{154}Gd [132]	0.55	0.55	−0.08	−1.00	−1.00	−0.12	0.24	0.90				−0.20	−0.10						
^{160}Gd [135]	0.42	0.42	−0.05	−0.80	−1.00	0.08	0.08	0.08				−0.20	−0.10						
^{160}Dy [135]	0.44	0.44	−0.06	−0.80	−0.90	0.08	0.08	0.08				−0.05	−0.15						
^{198}Pt [133]	0.58	0.58	−0.18	1.05	−0.80	−0.10	0.08	−0.10	0.00	0.02	0.00								
^{198}Hg [134]	0.55	0.55	−0.21	1.00	−0.40		0.08		0.37	0.25	0.16								
^{232}Th[a]	0.26	0.26	−0.05	−0.80	−1.45	0.20	0.20	0.20											
^{232}U[a]	0.28	0.28	−0.05	−1.00	−1.30	0.12	0.12	0.12				0.20	0.10						
^{238}U[a]	0.22	0.22	−0.05	−0.40	−1.30	0.12	0.12	0.12				0.20	0.10						
^{238}Pu[a]	0.24	0.24	−0.05	−0.60	−0.05	0.12	0.12	0.12		0.02			0.05	−0.09					

[a]Parameters fitted to reproduce the spectroscopic data of the low lying energy states.
[b]GS parameters fitted to reproduce the spectroscopic data of the low lying energy states.

TABLE XI. Single particle energies and isovector SDI strength parameters A_1 in MeV used for the 28–50 shell [66].

Orbital	Protons (particles) $A \sim 76$ $A_1 = 0.299$	Protons (holes) $A \sim 100$ $A_1 = 0.239$	Neutrons (holes) $A \sim 76$ $A_1 = 0.237$
$2p_{1/2}$	1.179	0.678	0.588
$2p_{3/2}$	0.000	1.107	1.095
$1f_{5/2}$	0.340	1.518	1.451
$1g_{9/2}$	2.640	0.000	0.000

TABLE XII. Single particle energies and isovector SDI strength parameters A_1 in MeV used for the 50–82 shell [66].

Orbital	Protons (particles) $A \sim 130$ $A_1 = 0.222$	Protons (particles) $A \sim 150$ $A_1 = 0.223$	Protons (holes) $A \sim 198$ $A_1 = 0.200$	Neutrons (particles) $A \sim 100$ $A_1 = 0.242$	Neutrons (holes) $A \sim 130$ $A_1 = 0.163$
$3s_{1/2}$	2.990	0.719	0.000	0.775	0.332
$2d_{3/2}$	2.440	0.466	0.350	1.142	0.000
$2d_{5/2}$	0.962	0.365	1.670	0.000	1.654
$1g_{7/2}$	0.000	0.000	2.700	0.172	2.434
$1h_{11/2}$	2.792	0.668	1.340	2.868	0.069

They include energies, B(E2) values, quadrupole moments, B(M1) values, magnetic moments, etc.. For the semimagic nuclei ^{124}Sn and ^{136}Xe, we have obtained the parameters by a fit to the energy of the low lying states using the same procedure as in Ref. [130] for ^{116}Sn. A compilation of the used parameters is given in Table X.

APPENDIX B: SURFACE DELTA INTERACTION STRENGTH VALUES A1 AND SINGLE-PARTICLE AND HOLE ENERGIES

The reliability of single-particle and -hole energies as well as the interaction strengths in connection with IBM-2 wave functions was studied in [66] by comparing recently measured occupation probabilities of initial and final states of interest in double beta decay. The pair structure constants were generated as usual by diagonalizing the surface delta interaction (SDI) in the two identical particle states, *pp*, *nn*, where the strength of the (isovector) interaction, A_1, is obtained by fitting the $2^+ - 0^+$ energy difference in nuclei with either two protons (proton holes) or two neutrons (neutron holes). The used single particle energies and A_1 values are given in Tables XI–XIV.

TABLE XIII. Single particle energies and isovector SDI strength parameters A_1 in MeV used for the 82–126 shell [66].

Orbital	Protons (particles) $A \sim 232$ $A_1 = 0.147$	Neutrons (particles) $A \sim 150$ $A_1 = 0.133$	Neutrons (holes) $A \sim 198$ $A_1 = 0.150$
$3p_{1/2}$	3.633	1.363	0.000
$3p_{3/2}$	3.119	0.854	0.900
$2f_{5/2}$	2.826	2.005	0.570
$2f_{7/2}$	0.896	0.000	2.340
$1h_{9/2}$	0.000	1.561	3.410
$1i_{13/2}$	1.608	3.700	1.630

TABLE XIV. SDI strength values A_1 and single particle energies (in MeV) in the $N = 126$–184 shell.

Orbital	Neutrons (particles) $A \sim 232$ $A_1 = 0.089$
$4s_{1/2}$	2.032
$3d_{3/2}$	2.538
$3d_{5/2}$	1.567
$2g_{7/2}$	2.491
$2g_{9/2}$	0.000
$1i_{11/2}$	0.779
$1j_{15/2}$	1.423

[1] E. W. Otten and C. Weinheimer, Rep. Prog. Phys. **71**, 086201 (2008).
[2] M. Aker *et al.* (KATRIN Collaboration), Phys. Rev. Lett. **123**, 221802 (2019).
[3] P. A. R. Ade *et al.* (Planck Collaboration), Astron. Astrophys. **594**, A13 (2016).
[4] P. Minkowski, Phys. Lett. **67B**, 421 (1977).
[5] R. N. Mohapatra and G. Senjanovic, Phys. Rev. Lett. **44**, 912 (1980).
[6] T. Yanagida, Conf. Proc. C **7902131**, 95 (1979).
[7] M. Gell-Mann, P. Ramond, and R. Slansky, Conf. Proc. C **790927**, 315 (1979).
[8] J. Schechter and J. W. F. Valle, Phys. Rev. D **22**, 2227 (1980).
[9] M. Agostini *et al.* (GERDA Collaboration), arXiv:2009.06079.
[10] H. Päs, M. Hirsch, H. Klapdor-Kleingrothaus, and S. Kovalenko, Phys. Lett. B **453**, 194 (1999).
[11] H. Pas, M. Hirsch, H. V. Klapdor-Kleingrothaus, and S. G. Kovalenko, Phys. Lett. B **498**, 35 (2001).

[12] F. del Aguila, A. Aparici, S. Bhattacharya, A. Santamaria, and J. Wudka, J. High Energy Phys. 05 (2012) 133.
[13] F. del Aguila, A. Aparici, S. Bhattacharya, A. Santamaria, and J. Wudka, J. High Energy Phys. 06 (2012) 146.
[14] Y.-H. Kim, arXiv:2004.02510.
[15] M. Doi *et al.*, Phys. Theor. Phys. **66**, 1739 (1983).
[16] M. Doi *et al.*, Phys. Theor. Phys. **69**, 602 (1983).
[17] T. Tomoda, Rep. Prog. Phys. **54**, 53 (1991).
[18] A. Ali, A. Borisov, and D. Zhuridov, arXiv:hep-ph/0606072.
[19] A. Ali, A. V. Borisov, and D. V. Zhuridov, Phys. Rev. D **76**, 093009 (2007).
[20] V. Cirigliano, W. Dekens, J. de Vries, M. Graesser, and E. Mereghetti, J. High Energy Phys. 12 (2017) 082.
[21] J. C. Helo, M. Hirsch, and T. Ota, J. High Energy Phys. 06 (2016) 006.
[22] F. F. Deppisch, T. E. Gonzalo, S. Patra, N. Sahu, and U. Sarkar, Phys. Rev. D **91**, 015018 (2015).
[23] F. F. Deppisch, C. Hati, S. Patra, P. Pritimita, and U. Sarkar, Phys. Rev. D **97**, 035005 (2018).
[24] V. Cirigliano, W. Dekens, J. de Vries, M. Graesser, and E. Mereghetti, J. High Energy Phys. 12 (2018) 097.
[25] G. Li, M. Ramsey-Musolf, and J. C. Vasquez, arXiv:2009.01257.
[26] F. F. Deppisch, L. Graf, J. Harz, and W.-C. Huang, Phys. Rev. D **98**, 055029 (2018).
[27] L. Graf, F. F. Deppisch, F. Iachello, and J. Kotila, Phys. Rev. D **98**, 095023 (2018).
[28] J. Barea and F. Iachello, Phys. Rev. C **79**, 044301 (2009).
[29] J. Barea, J. Kotila, and F. Iachello, Phys. Rev. C **87**, 014315 (2013).
[30] J. Barea, J. Kotila, and F. Iachello, Phys. Rev. C **91**, 034304 (2015).
[31] F. Šimkovic, A. Faessler, V. Rodin, P. Vogel, and J. Engel, Phys. Rev. C **77**, 045503 (2008).
[32] F. Šimkovic, V. Rodin, A. Faessler, and P. Vogel, Phys. Rev. C **87**, 045501 (2013).
[33] J. Suhonen, J. Phys. G **19**, 139 (1993).
[34] J. Suhonen, AIP Conf. Proc. **1488**, 326 (2012).
[35] E. Caurier, F. Nowacki, and A. Poves, Int. J. Mod. Phys. E **16**, 552 (2007).
[36] J. Menendez, A. Poves, E. Caurier, and F. Nowacki, Nucl. Phys. **A818**, 139 (2009).
[37] T. R. Rodriguez and G. Martinez-Pinedo, Phys. Rev. Lett. **105**, 252503 (2010).
[38] K. S. Babu and C. N. Leung, Nucl. Phys. **B619**, 667 (2001).
[39] A. de Gouvea and J. Jenkins, Phys. Rev. D **77**, 013008 (2008).
[40] J. C. Pati and A. Salam, Phys. Rev. D **10**, 275 (1974).
[41] R. N. Mohapatra and J. C. Pati, Phys. Rev. D **11**, 2558 (1975).
[42] G. Senjanovic and R. N. Mohapatra, Phys. Rev. D **12**, 1502 (1975).
[43] S. Dimopoulos and L. J. Hall, Phys. Lett. B **207**, 210 (1988).
[44] L. J. Hall and M. Suzuki, Nucl. Phys. **B231**, 419 (1984).
[45] R. N. Mohapatra, Phys. Rev. D **34**, 3457 (1986).
[46] M. Hirsch, H. Klapdor-Kleingrothaus, and S. Kovalenko, Phys. Rev. D **53**, 1329 (1996).
[47] S. L. Adler, E. W. Colglazier, J. B. Healy, I. Karliner, J. Lieberman, Y. J. Ng, and H.-S. Tsao, Phys. Rev. D **11**, 3309 (1975).
[48] S. Weinberg, Phys. Rev. **112**, 1375 (1958).
[49] M. R. Schindler and S. Scherer, Eur. Phys. J. A **32**, 429 (2007).
[50] F. Šimkovic, G. Pantis, J. D. Vergados, and A. Faessler, Phys. Rev. C **60**, 055502 (1999).
[51] V. Bernard, L. Elouadrhiri, and U.-G. Meissner, J. Phys. G **28**, R1 (2002).
[52] V. A. Andreev *et al.* (MuCap Collaboration), Phys. Rev. Lett. **110**, 012504 (2013).
[53] M. Gonzalez-Alonso, O. Naviliat-Cuncic, and N. Severijns, Prog. Part. Nucl. Phys. **104**, 165 (2019).
[54] J. Barea, J. Kotila, and F. Iachello, Phys. Rev. Lett. **109**, 042501 (2012).
[55] W. Haxton and G. Stephenson, Prog. Part. Nucl. Phys. **12**, 409 (1984).
[56] S. Weinberg, Nucl. Phys. **B363**, 3 (1991).
[57] V. Cirigliano, W. Dekens, J. de Vries, M. L. Graesser, E. Mereghetti, S. Pastore, and U. van Kolck, Phys. Rev. Lett. **120**, 202001 (2018).
[58] V. Cirigliano, W. Dekens, J. de Vries, M. L. Graesser, E. Mereghetti, S. Pastore, M. Piarulli, U. van Kolck, and R. B. Wiringa, Phys. Rev. C **100**, 055504 (2019).
[59] A. Arima, T. Ohtsuka, F. Iachello, and I. Talmi, Phys. Lett. **66B**, 205 (1977).
[60] F. Iachello and A. Arima, *The Interacting Boson Model* (Cambridge University Press, Cambridge, England, 1987).
[61] J. Barea, J. Kotila, and F. Iachello, Phys. Rev. C **87**, 057301 (2013).
[62] J. Kotila, J. Barea, and F. Iachello, Phys. Rev. C **89**, 064319 (2014).
[63] J. Barea, J. Kotila, and F. Iachello, Phys. Rev. D **92**, 093001 (2015).
[64] D.-L. Fang, A. Faessler, and F. Šimkovic, Phys. Rev. C **92**, 044301 (2015).
[65] T. Otsuka, A. Arima, and F. Iachello, Nucl. Phys. **A309**, 1 (1978).
[66] J. Kotila and J. Barea, Phys. Rev. C **94**, 034320 (2016).
[67] J. Engel, J. Phys. G **42**, 034017 (2015).
[68] G. A. Miller and J. E. Spencer, Ann. Phys. (N.Y.) **100**, 562 (1976).
[69] F. Šimkovic, A. Faessler, H. Muther, V. Rodin, and M. Stauf, Phys. Rev. C **79**, 055501 (2009).
[70] J. T. Suhonen, Front. Phys. **5**, 55 (2017).
[71] P. Puppe *et al.*, Phys. Rev. C **86**, 044603 (2012).
[72] F. Cappuzzello *et al.*, Eur. Phys. J. A **54**, 72 (2018).
[73] J. Menéndez, D. Gazit, and A. Schwenk, Phys. Rev. Lett. **107**, 062501 (2011).
[74] J. Menendez, A. Poves, E. Caurier, and F. Nowacki, J. Phys. Conf. Ser. **312**, 072005 (2011).
[75] A. Faessler, G. Fogli, E. Lisi, A. Rotunno, and F. Šimkovic, Phys. Rev. D **83**, 113015 (2011).
[76] J. Kotila and F. Iachello, Phys. Rev. C **85**, 034316 (2012).
[77] O. Azzolini *et al.*, Phys. Rev. Lett. **120**, 232502 (2018).
[78] J. Argyriades *et al.*, Nucl. Phys. **A847**, 168 (2010).
[79] R. Arnold *et al.* (NEMO-3 Collaboration), Phys. Rev. D **92**, 072011 (2015).
[80] A. S. Barabash *et al.*, Phys. Rev. D **98**, 092007 (2018).

[81] C. Arnaboldi *et al.*, Phys. Lett. B **557**, 167 (2003).
[82] D. Adams *et al.* (CUORE Collaboration), Phys. Rev. Lett. **124**, 122501 (2020).
[83] A. Gando *et al.* (KamLAND-Zen Collaboration), Phys. Rev. Lett. **117**, 082503 (2016).
[84] R. Arnold *et al.* (NEMO-3 Collaboration), Phys. Rev. D **94**, 072003 (2016).
[85] P. de Salas *et al.*, arXiv:2006.11237.
[86] V. Alenkov *et al.*, Eur. Phys. J. C **79**, 791 (2019).
[87] A. J. Zsigmond (LEGEND Collaboration), J. Phys. Conf. Ser. **1468**, 012111 (2020), https://iopscience.iop.org/article/10.1088/1742-6596/1468/1/012111/meta.
[88] S. R. Choudhury and S. Hannestad, J. Cosmol. Astropart. Phys. 07 (2020) 037.
[89] N. Mahajan, Phys. Rev. Lett. **112**, 031804 (2014).
[90] M. González, M. Hirsch, and S. G. Kovalenko, Phys. Rev. D **93**, 013017 (2016); **97**, 099907(E) (2018).
[91] M. Pavan (CUPID), J. Phys. Conf. Ser. **1468**, 012210 (2020), https://iopscience.iop.org/article/10.1088/1742-6596/1468/1/012210/meta.
[92] Y. Gando (KamLAND-Zen Collaboration), J. Phys. Conf. Ser. **1468**, 012142 (2020), https://iopscience.iop.org/article/10.1088/1742-6596/1468/1/012142/meta.
[93] A. Pocar (nEXO Collaboration), J. Phys. Conf. Ser. **1468**, 012131 (2020), https://iopscience.iop.org/article/10.1088/1742-6596/1468/1/012131/meta.
[94] A. Faessler, M. Gonzalez, S. Kovalenko, and F. Šimkovic, Phys. Rev. D **90**, 096010 (2014).
[95] P. D. Bolton, F. F. Deppisch, and P. B. Dev, J. High Energy Phys. 03 (2020) 170.
[96] Y. Cai, T. Han, T. Li, and R. Ruiz, Front. Phys. **6**, 40 (2018).
[97] A. Das, Adv. High Energy Phys. **2018**, 9785318 (2018).
[98] S. Mertens *et al.* (KATRIN Collaboration), J. Phys. G **46**, 065203 (2019).
[99] I. Krasnov, Phys. Rev. D **100**, 075023 (2019).
[100] C. Ahdida *et al.* (SHiP Collaboration), J. High Energy Phys. 04 (2019) 077.
[101] A. Blondel, E. Graverini, N. Serra, and M. Shaposhnikov (FCC-ee Study Team), Nucl. Part. Phys. Proc. **273–275**, 1883 (2016).
[102] S. Pascoli, R. Ruiz, and C. Weiland, J. High Energy Phys. 06 (2019) 049.
[103] S. Banerjee, P. S. B. Dev, A. Ibarra, T. Mandal, and M. Mitra, Phys. Rev. D **92**, 075002 (2015).
[104] S. Chakraborty, M. Mitra, and S. Shil, Phys. Rev. D **100**, 015012 (2019).
[105] A. Das, S. Jana, S. Mandal, and S. Nandi, Phys. Rev. D **99**, 055030 (2019).
[106] M. Nemevsek, F. Nesti, and G. Popara, Phys. Rev. D **97**, 115018 (2018).
[107] M. Aaboud *et al.* (ATLAS Collaboration), J. High Energy Phys. 01 (2019) 016.
[108] S. Mandal, M. Mitra, and N. Sinha, Phys. Rev. D **96**, 035023 (2017).
[109] F. F. Deppisch, M. Hirsch, and H. Päs, J. Phys. G **39**, 124007 (2012).
[110] W. Dekens, J. de Vries, K. Fuyuto, E. Mereghetti, and G. Zhou, J. High Energy Phys. 06 (2020) 097.
[111] C. Arbeláez, M. González, S. Kovalenko, and M. Hirsch, Phys. Rev. D **96**, 015010 (2017).
[112] P. Gysbers *et al.*, Nat. Phys. **15**, 428 (2019).
[113] J. M. Yao, B. Bally, J. Engel, R. Wirth, T. R. Rodríguez, and H. Hergert, Phys. Rev. Lett. **124**, 232501 (2020).
[114] A. Belley, C. Payne, S. Stroberg, T. Miyagi, and J. Holt, arXiv:2008.06588.
[115] S. Novario *et al.*, arXiv:2008.09696.
[116] J. Yao, arXiv:2008.13249.
[117] A. Faessler, S. Kovalenko, F. Šimkovic, and J. Schwieger, Phys. Rev. Lett. **78**, 183 (1997).
[118] G. Prezeau, M. Ramsey-Musolf, and P. Vogel, Phys. Rev. D **68**, 034016 (2003).
[119] T. Peng, M. J. Ramsey-Musolf, and P. Winslow, Phys. Rev. D **93**, 093002 (2016).
[120] F. F. Deppisch, J. Harz, M. Hirsch, W.-C. Huang, and H. Päs, Phys. Rev. D **92**, 036005 (2015).
[121] T. Otsuka and N. Yoshida, User's manual of the program NPBOS, Report No. JAERI-M 85-094, 1985.
[122] P. Duval, D. Goutte, and M. Vergnes, Phys. Lett. **124B**, 297 (1983).
[123] U. Kaup, C. Mönkemeyer, and P. V. Brentano, Z. Phys. A **310**, 129 (1983).
[124] U. Kaup and A. Gelberg, Z. Phys. A **293**, 311 (1979).
[125] H. Dejbakhsh, D. Latypov, G. Ajupova, and S. Shlomo, Phys. Rev. C **46**, 2326 (1992).
[126] P. V. Isacker and G. Puddu, Nucl. Phys. **A348**, 125 (1980).
[127] K.-H. Kim, A. Gelberg, T. Mizusaki, T. Otsuka, and P. von Brentano, Nucl. Phys. **A604**, 163 (1996).
[128] A. Giannatiempo, A. Nannini, A. Perego, P. Sona, and G. Maino, Phys. Rev. C **44**, 1508 (1991).
[129] M. Sambataro, Nucl. Phys. **A380**, 365 (1982).
[130] S. Cacciamani, G. Bonsignori, F. Iachello, and D. Vretenar, Phys. Rev. C **53**, 1618 (1996).
[131] O. S. G. Puddu and T. Otsuka, Nucl. Phys. **A348**, 109 (1980).
[132] O. Scholten, Ph.D. thesis, University of Groningen, 1980.
[133] R. Bijker, A. E. L. Dieperink, and O. Scholten, Nucl. Phys. **A344**, 207 (1980).
[134] A. F. Barfield, B. R. Barrett, K. A. Sage, and P. D. Duval, Z. Phys. A **311**, 205 (1983).
[135] J. Kotila, K. Nomura, L. Guo, N. Shimizu, and T. Otsuka, Phys. Rev. C **85**, 054309 (2012).